Journal of Advanced Research 86 (2026) 305–320

Contents lists available at ScienceDirect

Journal of Advanced Research

journal homepage: www.elsevier.com/locate/jare

Single-nucleus RNA sequencing illuminates a functional analog of lymphoid organ in crustacean

Mingzhe Sun [a,b,c], Shihao Li [a,b,c,*], Yuan Liu [a,b,c], Fuhua Li [a,b,c,**]

[a] State Key Laboratory of Breeding Biotechnology and Sustainable Aquaculture, Institute of Oceanology, Chinese Academy of Sciences, Qingdao 266000, China
[b] Laboratory for Marine Biology and Biotechnology, Qingdao Marine Science and Technology Center, Qingdao 266000, China
[c] Laboratory of Experimental Marine Biology, Institute of Oceanology, Chinese Academy of Sciences, Qingdao 266000, China

HIGHLIGHTS

- Macrophage-like and lymphocyte precursor-like cells were identified in Oka of shrimp.
- Macrophage-like cells in Oka express a mammalian NK/T cell marker ZAP-70 homolog.
- WSSV infection induces migration and aggregation of macrophage-like and lymphocyte precursor-like cells.
- Oka cells exhibit cytotoxic activity against heterologous cells.

GRAPHICAL ABSTRACT

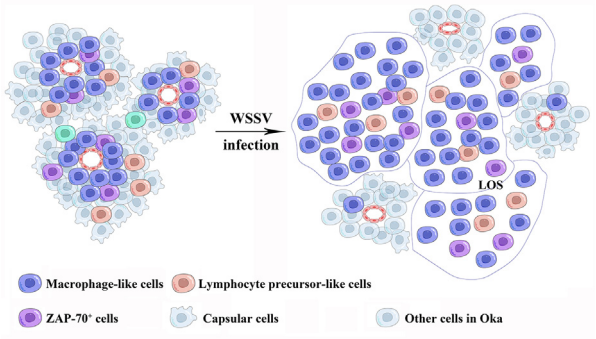

ARTICLE INFO

Article history:
Received 23 March 2025
Revised 10 October 2025
Accepted 12 November 2025
Available online 15 November 2025

Keywords:
Lymphoid organ
Macrophage-like cells
ZAP-70
Cytotoxic activity
Single-nucleus RNA-sequencing
Invertebrates

ABSTRACT

Introduction: The evolution of lymphoid organs is a complex topic in the animal kingdom. A presumptive invertebrate lymphoid organ (Oka) was previously reported in shrimp based on its morphological and histological observations. However, whether it truly functions as a lymphoid organ akin to those in vertebrates remains uncertain.
Objective: This study aims to characterize the cell composition of Oka at single-cell resolution and its function similarity with vertebrate lymphoid organs.
Methods: Single-nucleus RNA-seq and cross-species analysis were conducted to identify the major cell types in Oka of the whiteleg shrimp *L. vannamei*. The spatial expressions of the key genes were detected by *in-situ* hybridization and immunohistochemical analyses. Cytotoxic activity against heterologous cells was examined using fluorescence microscopy and flow cytometry.
Results: Oka comprised diverse cell types including ECM-producing cells, macrophage-like cells, lymphocyte precursor-like cells, capsular cells, hemocytes, SLC-rich cells, epithelial cells and progenitors. Notably, typical vertebrate macrophage markers (NLRP3, LAMP2 and LGMN) and ZAP-70, a marker of T lymphocytes/natural killer (NK) cells were expressed in the macrophage-like cells. The lymphocyte precursor-like cells, characterized by the expression of YBX3 and SOX4, were further distinguished by the up-regulated expression of CD39, CD49d, and CD133 homologues following WSSV infection. These two cell types were observed to migrate into the lymphoid organ spheroid during structural remodeling of the Oka following WSSV infection. Functionally, Oka cells of shrimp also exhibited cytotoxic activity against heterologous cells.

* Corresponding author at: State Key Laboratory of Breeding Biotechnology and Sustainable Aquaculture, Institute of Oceanology, Chinese Academy of Sciences, Qingdao 266000, China.
** Corresponding author at: State Key Laboratory of Breeding Biotechnology and Sustainable Aquaculture, Institute of Oceanology, Chinese Academy of Sciences, Qingdao 266000, China.
E-mail addresses: lishihao@qdio.ac.cn (S. Li), fhli@qdio.ac.cn (F. Li).

https://doi.org/10.1016/j.jare.2025.11.018

Conclusion: The presence and WSSV infection-induced aggregation of ZAP-70 positive cells in Oka of shrimp and its cytotoxic activity against heterologous cells suggest that shrimp Oka might perform similar function as the lymphoid organ in vertebrates. The present results will not only provide evidence to confirm the function of Oka in shrimp, but also greatly widen the knowledge about the origin and evolution of lymphoid organ in the animal kingdom.

Introduction

Multicellular organisms have evolved complex defense mechanisms to ensure survival against infections. Persistent pathogen pressure drives the evolutionary emergence of specialized immune cells, tissues and organs that facilitate effective immune responses. Lymphoid organs are important regulators that govern lymphocyte development and immune responses [1]. Mammals have evolved the specialized primary and secondary lymphoid organs or tissues, which serve as the functional cornerstone of adaptive immunity. Primary lymphoid organs, such as thymus and bone marrow, provide specialized microenvironments to foster the generation of B and T lymphocytes. The secondary lymphoid tissues, including spleen, lymph nodes, and mucosa-associated lymphoid tissue (MALT) *etc.* specialize in the coordination of immune responses [2].

The emergence and diversification of lymphoid organs or tissues constitute a compelling evolutionary topic across metazoans. The primary lymphoid organs emerge in early vertebrates, while the appearance of secondary lymphoid tissues exhibit species-specific variability [3]. The development of B cell is conserved within hematopoietic niches across all vertebrates. Hematopoietic tissues usually exhibit gut-associated localization, such as the lamprey typhlosole, the shark Leydig's organ, and the epigonal organ in cartilaginous fishes [4]. The ancient primary lymphoid organ thymus governs T cell development and occupies pharyngeal or cervical regions across vertebrates [5]. Mucosal surfaces serve as pivotal interfaces with the external environments. Their constant exposure to pathogens drives the evolution of specialized mucosal-associated lymphoid tissues (MALTs). Teleost deploys multiple MALTs to protect their barrier surfaces, including the gut-associated (GALT), the skin-associated (SALT), the nasal-associated (NALT), and gill-associated lymphoid tissues (GIALT) [6]. Owing to the absence of somatically diversified antigen receptors and well-differentiated lymphocyte lineages, invertebrates are generally regarded as lacking lymphoid organs.

In crustaceans, a lymphoid organ (Oka) was reported with lymph-like cells surrounded by lymphoid interstitial tissues [7]. It comprises a pair of lobes surrounded by connective tissues. Each lobe contains numerous tubules with central lumens, endothelial cells and matrix cells. Haemal sinuses occupy the inter-tubular spaces [8]. Constitutively, various immune-related molecules, including antimicrobial peptides and the prophenoloxidase system molucules, are expressed in Oka [9]. Viral infection to shrimp triggers structural remodeling within this organ, that is the formation of cell aggregates termed lymphoid organ spheroid (LOS) [10]. It exhibits morphological and pathological similarities to lymphoid tissues like nemausean lymphoid organ in fish [11]. However, whether it truly functions as a lymphoid organ similar to those in vertebrates remains uncertain and warrants investigation.

The advent of single-cell and single-nucleus RNA sequencing (scRNA-seq & snRNA-seq) technology enable to resolve transcriptional landscapes at single-cell resolution. This technology has been widely employed to characterize the cell lineage heterogeneity in various crustacean tissues, including hepatopancreas, hemocytes, and hematopoietic tissues [12–15]. Here, we performed snRNA-seq on the presumptive lymphoid organ (Oka) of the marine invertebrate *Litopenaeus vannamei*, and characterized the immune functions of major cell types to trace its functional similarity with vertebrate lymphoid organs. The study identified 16 types of cells in Oka, among which macrophage-like cells (37.20%), ECM producing cells (26.87%) and lymphocyte precursor-like cells (7.45%) occupied the majority. White spot syndrome virus (WSSV) infection induced cell migration and aggregation in Oka were detected by *in-situ* hybridization and immunohistochemical analyses. The cytotoxic activity of Oka cells was characterized via functional assay. Our study indicates that Oka in shrimp exhibits similar functions with lymphoid organs in vertebrates, which provides critical insights into the evolutionary origins of lymphoid organ in the animal kingdom.

Materials and methods

Experimental animals and viral challenge

Healthy shrimp with an average body weight of 13.0 ± 1.1 g were acclimated for 7 days in aerated seawater (25 ± 1 °C) prior to tissue collection and WSSV challenge. WSSV particles were prepared according to the method described by Sun et al. [16]. The virus particles at a final concentration of 3000 copies per individual was diluted in 10 μL sterilized phosphate buffered saline (PBS). The diluted viruses were administered via abdominal injection (segments III–IV) to the shrimp in the WSSV group. At 24 h post-infection (hpi), the Oka from 20 infected individuals were pooled as one sample for WSSV group. At the same time, the Oka from 20 healthy individuals without any treatment were pooled as a control sample. The samples were immediately preserved in liquid nitrogen for snRNA-seq.

Single-nucleus extraction, encapsulation and sequencing

SnRNA-seq procedures, including nucleus isolation, droplet encapsulation, library synthesis and processing of sequenced raw data, were conducted by Gene Denovo (Guangzhou, China) following established protocols. In brief, nucleus suspensions of shrimp Oka were processed using the Chromium Single Cell 3′ Gel Bead-in Emulsion, Library and Gel Bead Kit (10 × Genomics) to generate the barcoded snRNA-seq libraries according to the manufacturer's protocol. Then, the library quantification was conducted using KAPA Library Quantification Kit (KAPA Biosystems) and Agilent Bioanalyzer 2100. Finally, library sequencing was performed on Illumina HiSeq 4000 with paired-end configuration (Read 1: 26 bp, read 2: 98 bp).

SnRNA-seq data processing and analysis

Raw sequencing data were processed using Cell Ranger Suite (v6.1) for demultiplexing, barcode/UMI correction, and gene quantification. Initial demultiplexing of Illumina base calls to FASTQ files was performed with bcl2fastq, followed by quality assessment using FastQC. Reads were aligned to the *L. vannamei* genome (NCBI TaxID: 6689) via STAR aligner. Then, the low-quality sequences (invalid barcodes/UMIs, PCR duplicates) were filtered using Cell Ran-

ger "count" module. Low-quality cells were excluded using Seurat (v4.0.4) with stringent thresholds (genes/cell > 3,000, UMIs/cel l > 12,000, and mitochondrial gene content > 15%).

Canonical correlation analysis (CCA) was used to normalize the gene-barcode matrix prior to UMAP visualization. A graph-based clustering algorithm identified 16 transcriptionally distinct cell clusters in Oka based on expression pattern of marker genes. Cluster-specific gene enrichment was determined through median expression profiling across all cells in each cluster. Gene set enrichment analysis (GSEA) was performed to characterize the antiviral responses in healthy versus WSSV-infected Oka with criteria (NES < –1 or NES > 1, FDR < 0.25, $p < 0.05$). Differentially expressed genes (DEGs) were identified with criteria ($p \leq 0.01$, log2FC ≥ 0.36, and detection rate in target cluster > 25%). The identified DEGs were visualized through Seurat-generated heatmaps.

Monocle 2 (v2.6.4) was used to reconstruct differentiation trajectories using differentiation and cell fate-related genes based on the previously identified cell clusters and DEGs. Major cells in Oka-0h were assigned as start point and cells were ordered in the two reduced dimensions to visualize the trajectory of cells in Oka upon viral infection. Bioinformatic analysis was conducted, and related images were generated using Omicsmart (http://www.omicsmart.com) and OmicShare Tools [17].

AlphaFold3 models

The tertiary structures of human ZAP-70 and its homolog in shrimp (LvZAP-70) were predicted using the AlphaFold3 server [18] under default parameters. The highest-confidence models (ranked as model 0) from five predicted conformations considering the pLDDT scores were selected for structural visualization by Pymol 2.5.0.

In-situ hybridization

T7 promoter-linked primers (Supplementary Table S1) were used to amplify the DNA templates of cluster-specific markers for antisense/sense probes synthesis. The DNA templates were purified using MiniBEST DNA Fragment Purification Kit (Takara, Japan) followed by electrophoretic validation (1.5% agarose). Digoxygenin (DIG)-labeled riboprobes were generated via *in vitro* transcription using TranscriptAid T7 High Yield Transcription Kit (Thermo Fisher Scientific, USA) with DIG RNA Labeling Mixture (Roche, Germany). Probe integrity was confirmed through Nanodrop 2000 quantification (Thermo Fisher Scientific, USA) and electrophoretic analysis before storage at –80 °C.

The Oka samples from healthy and WSSV-infected shrimp were fixed in 4% paraformaldehyde at 4 °C for 24 h. They were then dehydrated in 75%, 80%, 95% and 100% ethanol. The samples were cleared with xylene and embedded in paraffin wax. The sections (7 μm) were prepared, then deparaffinated in xylene and rehydrated in diluted ethanol series from 95% up to RNase-free water. Then, the rehydrated sections underwent hybridization with antisense riboprobes (1 ng/μL each) according to the general protocol of DIG RNA labeling kit (Roche, Germany). Finally, the signals were visualized through Nikon Eclipse 80i microscope (Nikon, Japan) after reaction with NBT/BCIP Stock Solution (Roche, Germany). The same amount of sense riboprobes was used for control sections under the same procedure.

Immunohistochemical detection

The above sections were deparaffinated in xylene, rehydrated through a graded ethanol series, starting from 95% and proceeding to distilled water. The antigen was retrieved by refolding in sodium citrate-hydrochloric acid buffer. Then, the slides were blocked with 3% bovine serum albumin (BSA) in PBS at room temperature for 1 h. They were subsequently incubated with 1:200 diluted rabbit anti-ZAP-70 monoclonal antibody (99F2, Cell Signaling Technology, USA) at 4 °C overnight. The slides were then washed with PBS containing 0.05% Tween-20 (PBST). The sections were incubated with 1:500 diluted Alexa Fluor 488-labeled goat-anti-rabbit secondary antibody (HA1121, Huabio, China) at room temperature for 1 h. Then, the slides were washed again with PBST and mounted with coverslips using antifade mounting medium with DAPI (P0131, Beyotime, China). Finally, the signals were visualized under a laser confocal scanning microscopy (LSM 900, Carl Zeiss, Germany).

RNA interference (RNAi)

Pairs of primers with T7 promoter sequence (Supplementary Table S1) were used to clone DNA fragment of *LvZAP-70* and enhanced green fluorescent protein (EGFP) genes for double-stranded RNA (dsRNA) synthesis. The synthesis and purification of dsRNA were conducted as previously described [19]. Different dosages of dsRNA were injected into each shrimp to optimize its silencing efficiency. Ninety shrimp with an average body weight of 8.4 ± 0.2 g were randomly separated into dsEGFP and dsZAP70 group, and each group contained 45 shrimp. After detecting the silencing efficiency, the dosage of 0.50 μg/g *LvZAP-70* dsRNA was used for RNAi experiment in the dsZAP70 group. Shrimp in the dsEGFP group received the same amount of EGFP dsRNA. At 48 h post dsRNA injection, Oka tissues from two groups were harvested for further extraction and incubation, respectively.

Cytotoxicity assay of Oka cells

Heterologous cells including HEK293T cells, S2 cells and Sf9 cells were selected to carry out the cytotoxicity assay. HEK293T cells were maintained in DMEM supplemented with 10% FBS at 37 °C/5% CO_2. *Drosophila* S2 cells were maintained in SFX-Insect™ medium supplemented with 10% FBS at 27 °C. Sf9 cells were maintained in Sf-900™ II SFM medium at 27 °C. Primary culture cells of shrimp Oka were prepared as adherent monolayers in 12-well cell plates at 27 °C using a kind of culture medium developed in our lab. The culture medium mainly contains the modified L-15 medium supplemented with 15% FBS and 10% shrimp muscle extract. For co-culture assays, 2×10^5 non-adherent *Drosophila* S2 cells were introduced to Oka cell monolayers and incubated at 27 °C for 24 h in the co-culture group. The cell culture plates were gently shaken to collect supernatant containing S2 cells after incubation. The harvested S2 cells were washed three times with PBS and stained with propidium iodide (PI, C1062M, Beyotime, China) for 20 min at room temperature. Cell viability was quantified via flow cytometry (FACSAria II, BD, USA), with PI-high populations (intensity $>2 \times 10^3$) designated as dead cells according to the pre-test result. S2 cells cultured identically without Oka cells were served as negative control.

Oka and partial muscle tissues (0.5 g each) from healthy shrimp were homogenized separately in ice-cooled sterile PBS (3 mL/g tissue) using mechanical disruption. Half of the Oka homogenate underwent heat inactivation at 70 °C for 1 h with intermittent shaking, while the muscle homogenate and the remnant of Oka homogenate were maintained at 4 °C. All homogenates were centrifuged at 8,000 rpm at 4 °C for 30 min. Then the supernatants were filter-sterilized (0.22 μm) and stored at –80 °C until subsequent applications. Oka tissues from shrimp in dsEGFP and dsZAP70 groups were homogenized and filter-sterilized as previously described without heat inactivation. Heterologous cells were seeded in 12-well cell culture plates under standardized densities. For the healthy Oka extract, heterologous cells of each type were

divided into four treatment groups: one receiving 10% (v/v) sterile PBS (negative control group), another was added with 10% muscle extract (muscle extract group), a third was added with 10% heat-inactivated Oka extract (heated Oka extract group), and the fourth was added with 10% native Oka extract (Oka extract group). For the Oka extract following gene knock-down, heterologous cells of each type were divided into three treatment groups: one receiving 10% (v/v) sterile PBS (negative control group), another was added with 10% Oka extract of shrimp from dsEGFP group (Oka extract in dsEGFP group), and the third was added with 10% Oka extract of shrimp from dsZAP70 group (Oka extract in dsZAP70 group). Following 24-hour incubation, cells were washed with PBS and stained using the Cell Viability/Cytotoxicity Assay Kit (C2015, Beyotime, China). Live and dead cell distributions were observed via fluorescence microscopy, while quantitative cell death assessment for S2 and Sf9 cells was performed by flow cytometry using PI staining following the established protocols.

Plasmid construction and transfection

The open reading frame (ORF) of *LvZAP-70* was amplified using specific primers (Supplementary Table S1) and inserted into the pEF1α/Myc-his vector (Youbio, China) using In-Fusion HD Cloning Plus (Clontech, Mountain View, CA, USA). Jurkat, Clone E6-1 cells were cultured in RPMI 1640 medium supplemented with 10% FBS at 37 °C/5% CO_2. Plasmids were transfected into Jurkat cells using ProteanFect Max Transfection Kit (Nanoportal Biotech, China) according to the manufacturer's instructions. At 48 h post transfection, the cells were harvested for subsequent RNA extraction and detection.

Quantitative Real-time PCR (qPCR) and RT-PCR detection

Tissue collection, RNA extraction, and cDNA synthesis were described previously [19]. qPCR was performed to profile the spatiotemporal expression of *LvZAP-70*, human *ZAP-70*, *CD69*, *CD25*, and *IL-2* (Supplementary Table S1) across different samples. Amplification specificity was verified through melting-curve analysis. Human *GAPDH* and shrimp *18S rRNA* (Supplementary Table S1) were employed as internal references for cDNA normalization of Jurkat cells and shrimp tissue samples, respectively. RT-PCR was conducted to analyze the expression of *LvZAP-70* in Jurkat cells after transfection as previously described [19]. The amount of cDNA templates from Jurkat cells was quantified using human *GAPDH* as an internal reference gene. An equal amount of cDNA from different Jurkat cells was used for detecting the expression pattern of *LvZAP-70* transcripts. The PCR products were detected by electrophoresis on 2% agarose gel.

Statistical analysis

Data were expressed as mean ± SEM derived from three biological replicates. Statistical comparisons between groups were conducted using independent sample *t*-tests in SPSS 19.0 (IBM, USA), with significance thresholds set at $^{*}p < 0.05$ and $^{**}p < 0.01$.

Results

SnRNA-seq clustering of major cell types in Oka

Histological observation indicated that WSSV infection led to structural remodeling in shrimp Oka at 24 hpi, notably the formation of LOS in comparison with Oka from healthy shrimp (Supplementary Fig. S1). To resolve cellular heterogeneity in Oka, we performed snRNA-seq analysis using 10 × Genomics platform on the cell nuclei isolated from Oka of healthy shrimp (Oka-0h) and those from WSSV-infected shrimp at 24 hpi (Oka-24h-WSSV) (Fig. 1A). After quality control, a total of 27,049 cells (13,265 cells from Oka of healthy shrimp sample and 13,784 cells from Oka of WSSV-infected shrimp sample) were classified into 16 transcriptionally distinct clusters (Supplementary Fig. S2A), ranging in size from the maximal cluster 0 (26.84%) to the minimal cluster 15 (0.19%).

Annotations of marker genes were used to define the cell types and their potential functions in Oka (Fig. 1B). Six clusters (cluster 0, 1, 2, 5, 7, and 13) were annotated based on the known functions of top five marker genes. Cluster 0, enriched in *elastin* (cross-linked protein for ECM elasticity regulation) [20] and *extensin* (cross-linking glycoprotein for structural reinforcement) [21,22], was designated as ECM-producing cells. Cluster 1 and 2, were classified as macrophage-like cells based on the high expressions of macrophage-associated markers, such as *Solute Carrier Family 46 Member* (*SLC46A*, a dominant cGAMP importer in macrophages) [23], *Legumain* (*LGMN*, a phagocytic proteinase primarily in macrophages) [24,25], and *NOD-like receptor protein 3* (*Nlrp3*, an inflammasome component in macrophages). *TRIM9-1* is a marker of cluster 5, which is specifically expressed in the lymphoid tubules of Oka [19]. Combined with their spatial distribution (Supplementary Fig. S3), cluster 5 was designated as capsular cells. Cluster 7 was identified as hemocytes based on the presence of hemocyte-specific markers, including *transglutaminase* (*TGMN*) and *prophenoloxidase-3* (*PPO3*) [26,27]. The marker genes involved in mitotic processes, including *transforming acidic coiled-coil-containing protein 3* (*TACC3*), *centrosome-associated protein E* (*CENPE*), *Cyclin B3* (*CCNB3*), and *abnormal spindle-like microcephaly-associated protein* (*ASPM*), highly expressed in cluster 13. Further analysis revealed that most cells in cluster 13 stayed at the mitosis phase (with a higher percentage of G2 and M phases) (Supplementary Fig. S4). Therefore, cluster 13 was identified as progenitor cells.

For clusters with unknown marker gene functions, we referenced their vertebrate homologs to define the cell subsets [14]. We summarized the top 50 differentially expressed genes (DEGs) for each cluster, identified their vertebrate homologs, and analyzed their expression across major human cell types using the Human Cell Atles database [28]. In addition to the known markers used to annotate cluster 1 and 2 as described above, we further utilized their top 50 marker genes for validation. In cluster 1 and 2, we identified additional macrophage marker homologs, including *palmitoyl-protein thioesterase 1* (*PPT1*), *Insulin-Like Growth Factor 2 Receptor* (*IGF2R*), *carboxypeptidase vitellogenic-like* (*CPVL*), *phospholipase A2* (*PLA2*), *multiple EGF like domains 10* (*MEGF10*), and *solute carrier family 22 member 3* (*SLC22A3*) (Tables S2, S3) [29,30]. Given the high correlation between these subsets (Supplementary Fig. S2B, correlation: 0.995), we merged cluster 1 and 2 as a single cell type, categorized as macrophage-like cells. In cluster 4, we detected several homologs of lymphocyte-associated genes, including *Y-box binding protein 3* (*YBX3*), *SRY-box transcription factor 4* (*SOX4*), and *lysosomal trafficking regulator* (*LYST*) (Table S4). YBX3 is a known marker of pre-B cell differentiation [31]. LYST regulates lytic granule dynamics in cytotoxic T-cells and natural killer (NK) cells by controlling granule size, number and exocytosis [32]. SOX4 governs T cell maturation and development via binding to the T cell enhancer motif (5′-AACAAAG-3′ motif) [33,34]. Since invertebrates lack differentiated B cells, T cells, or other adaptive immunity-related lymphocytes, cluster 4 likely represents pro- or pre-lymphocyte homologs. Thus, we designated this cluster as lymphocyte precursor-like cells. The majority of DEGs in cluster 8 belonged to the solute carrier (*SLC*) family (Table S5), thus we named them as SLC-rich cells. When comparing the top 50 DEGs of cluster 11 with human homologs, we identified several genes,

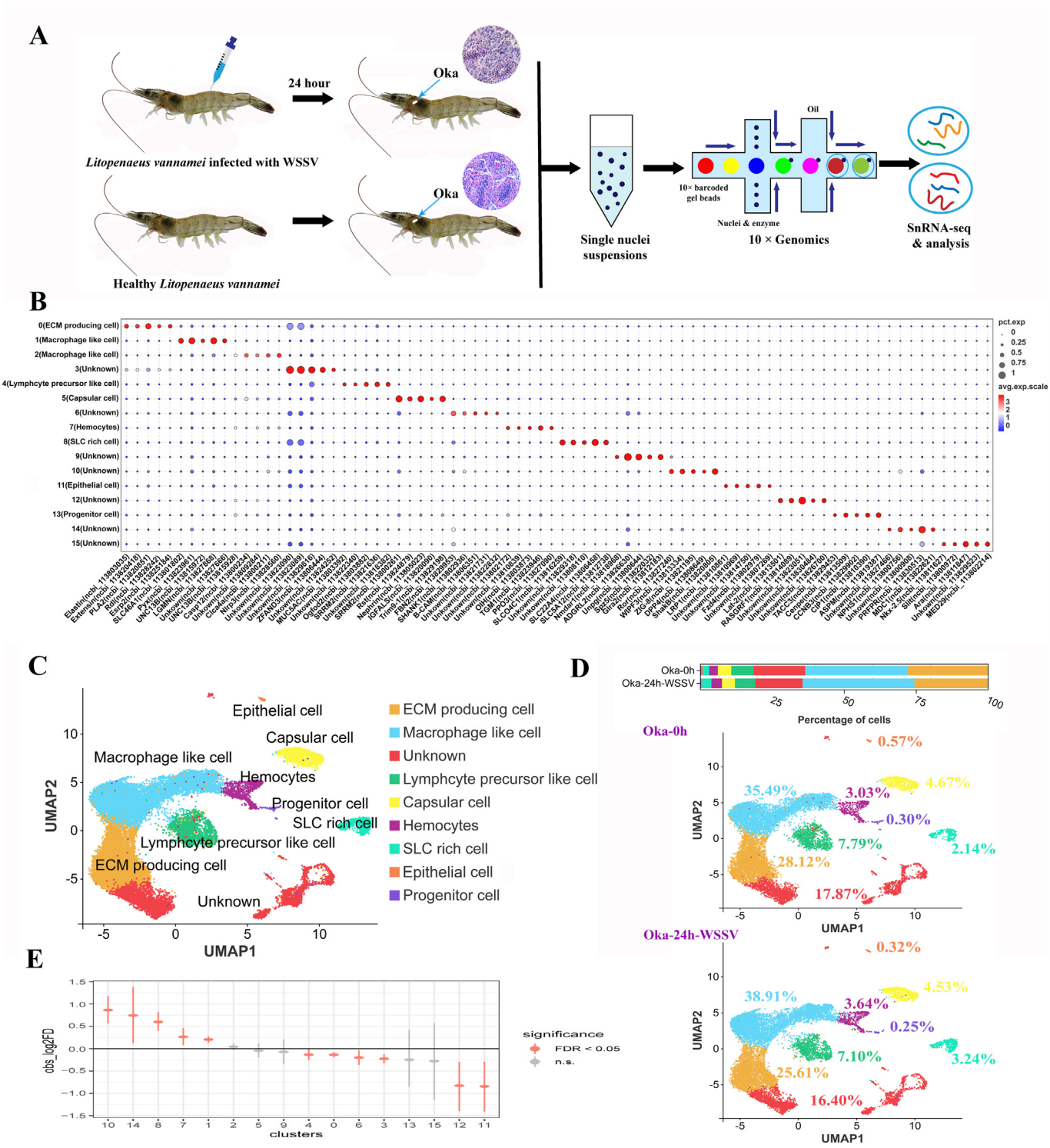

Fig. 1. Single-nucleus profiling of cell populations in the lymphoid organ (Oka) of shrimp. (A) Schematic illustration of the experimental workflow. The Oka samples were collected from WSSV-infected shrimps at 24 hpi and healthy shrimp, with 20 Oka samples from each group pooled together as one sample for single-nucleus RNA sequencing (snRNA-seq) analysis. The position of Oka within shrimp was marked with arrows, and its morphological features under different conditions were shown. (B) A dot plot displaying representative marker genes for each cluster. The gene names and their NCBI GeneIDs are listed at the bottom, while the clusters and their annotated cell types are listed on the left. Dot size represents the fraction of cells in the cluster that express each gene, and colors indicate the mean expression in expressing cells relative to other clusters. (C) A Uniform Manifold Approximation and Projection (UMAP) plot illustrating the major cell types identified in snRNA-seq dataset. (D) Proportions of the cell types for each treatment are shown in a stack chart (top) and UMAP plots (middle and bottom). (E) Changes of cell proportions between these groups using scProportion tools with FDR < 0.05.

including *reelin*, *laminin*, *hemicentin 1*, *plexin A1* (Table S6), that are specifically expressed in human endothelial cells (e.g., lymphatic endothelial cells). Combined with their spatial distribution (Supplementary Fig. S3), cluster 11 was annotated as epithelial cells. The remaining clusters lacked definitive immune-related homologs and were thus categorized as unknown cells.

Based on the annotation of top 50 DEGs, we constructed a cellular atlas of Oka in penaeid shrimp (Fig. 1C). ECM-producing cells and macrophage-like cells account for the majority of the cell populations in Oka (Fig. 1D), which aligns with its previously reported tissue architecture and immune functions.

In order to know the immune response of different clusters in Oka, we analyzed the variations of cell numbers in different clusters of Oka when shrimp was infected by WSSV. We found that the proportions of cells in cluster 0, 3, 4, 6, 11, and 12 decreased significantly, whereas those in cluster 1, 7, 8, 10, and 14 increased significantly following WSSV infection (Fig. 1E, Supplementary Fig. S5).

Immunological function characterization of different clusters

Based on previously reported shrimp immune-related genes [35–37], we analyzed their expression levels in the above identified 16 clusters to further elucidate their diverse immunological functions.

Phagocytosis acts as a pivotal defense mechanism for clearing bacterial and viral pathogens. Given the multitude of molecules involved in this complex process, pinpointing the predominant phagocytic cluster in Oka is challenging. However, several phagocytosis-related genes exhibited relatively high expression levels in clusters 1 and 2 (Fig. 2A). In eukaryotic cells, intra- and extracellular macromolecules are primarily degraded by lysosomal components and associated enzymes [38]. Abnormal lysosomes can seriously impair the antiviral capability of shrimp [39]. Analysis of DEGs revealed that cluster 1 exhibited a significantly elevated expression of lysosome related genes (Fig. 2B), including *lysosomal associated membrane protein 1* (*lamp1*), lgmn, *cathepsin* (*CST*), *cluster of differentiation antigen 63* (*CD63*), *sphingomyelin phosphodiesterase 1* (*SMPD1*). These findings suggested that the tissue-specific macrophage-like cells in Oka might possess a robust ability for engulfing and degrading foreign materials.

Programmed cell death (PCD) is a complex process essential for maintaining cellular homeostasis and mediating immune defense. In crustaceans, apoptosis, necroptosis, autophagy-dependent cell death, and ferroptosis are critical PCD events for defense to pathogen [35]. Autophagy is a process that renews specific cellular components through degradation by autophagic lysosomes. It can lead to cell death under certain conditions. *GABA type A receptor-associated protein* (*GABARAP*), a hallmark of canonical autophagy, was specifically expressed in cluster 8 in Oka (Fig. 2C). Some autolysosomal components (which are shared with lysosome) showed relatively higher expression in cluster 1. NOD-like receptor (NLR)-mediated apoptosis participates in the antibacterial and antiviral immunity in shrimp [40]. Several *caspases* and NLR pathway related genes were highly expressed in cluster 2 and 8 (Fig. 2D and Supplementary Fig. S6). Ferroptosis, an iron-dependent cell death, plays a crucial role in lipid peroxidation and immune responses [41]. *SLC40A1* (also known as *ferroportin-1*), *acyl-CoA synthetase long-chain family 4* (*ACSL4*), *glutathione synthetase* (*GSH2*), and several other ferroptosis related genes were highly expressed in cluster 8 (Fig. 2E). Various necroptosis-related genes exhibited high expression levels in cluster 1, 8 &13 (Fig. 2F).

The Toll and immune deficiency (IMD) pathways are two major signaling cascades mediating humoral immune responses in shrimp. Upon recognition of pathogens by pattern recognition receptors, downstream signaling transduction is triggered to activate the transcription of immune effectors. Key components of these two pathways, including the receptors (*toll-7* and *toll-9*), the ligand *Spätzle* (*Spz*), and the transcription factors *relish* (*Rel*) and *dorsal*, were highly expressed in cluster 5, 7 and 11 (Fig. 2G). Antimicrobial peptides (AMPs) are pivotal effectors of invertebrate immunity, and most of them are produced in hemocytes and Oka in shrimp. Expression profiles revealed that *crustin IIa* and *stylicines* were highly expressed in cluster 7, while *anti-lipopolysaccharide factors* (*ALF*s) were highly expressed in cluster 5 (*ALF8*, *ALF-AVR*) and cluster 9 (*ALF4*, *ALF6*) (Fig. 2H). Melanization, a prophenoloxidase (PPO) activation cascade comprising pattern recognition proteins, several serine proteases and their inhibitors, is critical for wound healing and clearance of invading pathogens. We found that most PPO-related genes were relatively highly expressed in cluster 7, including the zymogen *PP3*, the activators *prophenoloxidase activating factors 2* (*PPAF2*), *prophenoloxidase-activating enzyme* (*PPAE*), and the inhibitor *Kunitz-type protease inhibitor* (*KTPI*) (Fig. 2I). The high expression of the PPO-activation system in these cells aligns with their identification as hemocytes. The Vago-JAK-STAT pathway is an analog of interferon (IFN)-induced antiviral signaling in arthropods [42]. The homolog of IFN, components of JAK-STAT pathway, and IFN-stimulated genes were expressed across various types of Oka cells, with relatively higher expression levels in cluster 5 and 7 (Fig. 2J). These data collectively indicated that cluster 5 and 7 might play key roles in mediating humoral immune responses in shrimp.

Macrophage-like cells migrated from lymphoid tubules to LOS following WSSV infection in Oka

Oka functions as a primary phagocytic tissue in penaeid shrimp, and our data revealed the presence of macrophage analogs within this tissue. Following WSSV infection, the proportion of macrophage-like cells increased (Fig. 1D, E), highlighting their essential roles in antiviral defense. We further analyzed the molecular features, spatial distribution and antiviral responses of macrophage-like cells. The homologs of conserved macrophage markers, including *CD36* and *galectin-3*, were highly expressed in macrophage-like cells (Table S7). Cross-species comparisons revealed that both conserved macrophage markers (Fig. 3A) and evolutionary/species-specific macrophage markers (Supplementary Fig. S7) across multiple vertebrates were predominantly expressed in macrophage-like cells. Previous identified invertebrate homologs of human macrophages [14] were mainly expressed in macrophage-like cells (Supplementary Fig. S8A). These results further suggested the existence of tissue-specific macrophage-like cells in Oka. However, subtle differences in immune function distinguished the subpopulations, and we designated them as macrophage-like cell 1 (cluster 1) and macrophage-like cell 2 (cluster 2) (Supplementary Fig. S9). Enrichment analysis revealed that genes related to the engulfment and degradation of foreign materials, particularly lysosomal components were highly expressed in macrophage-like cell 1. In contrast, genes involved in cytokine receptor-mediated signaling transduction, including subunits of G-proteins and NF-κB/STAT transcription factors were highly expressed in macrophage-like cell 2 (Fig. 3B).

To characterize the spatial distribution and function of macrophage-like cells during viral infection, we performed *in-situ* hybridization on Oka from healthy and WSSV-infected shrimp. As previously described, the Oka of shrimp comprised numerous lymphoid tubules, which contained three major cell types: endothelial (En) cells in the inner layer, stromal (St) cells in the middle layer, and capsular (Cp) cells in the outer layer under histological observation (Supplementary Fig. S1). *In-situ* hybridization revealed that the positive signals for cluster 1 and 2 markers were similarly located in the middle layer of the lymphoid tubules in Oka of healthy shrimp. Following WSSV infection, these positive signals translocated to cell aggregation in the inter-tubular space, the location of LOS in Oka (Fig. 3C).

Pseudotime analysis using Monocle 2 was performed to reconstruct the differentiation trajectory of macrophage-like cells following WSSV infection. WSSV infection induced a novel

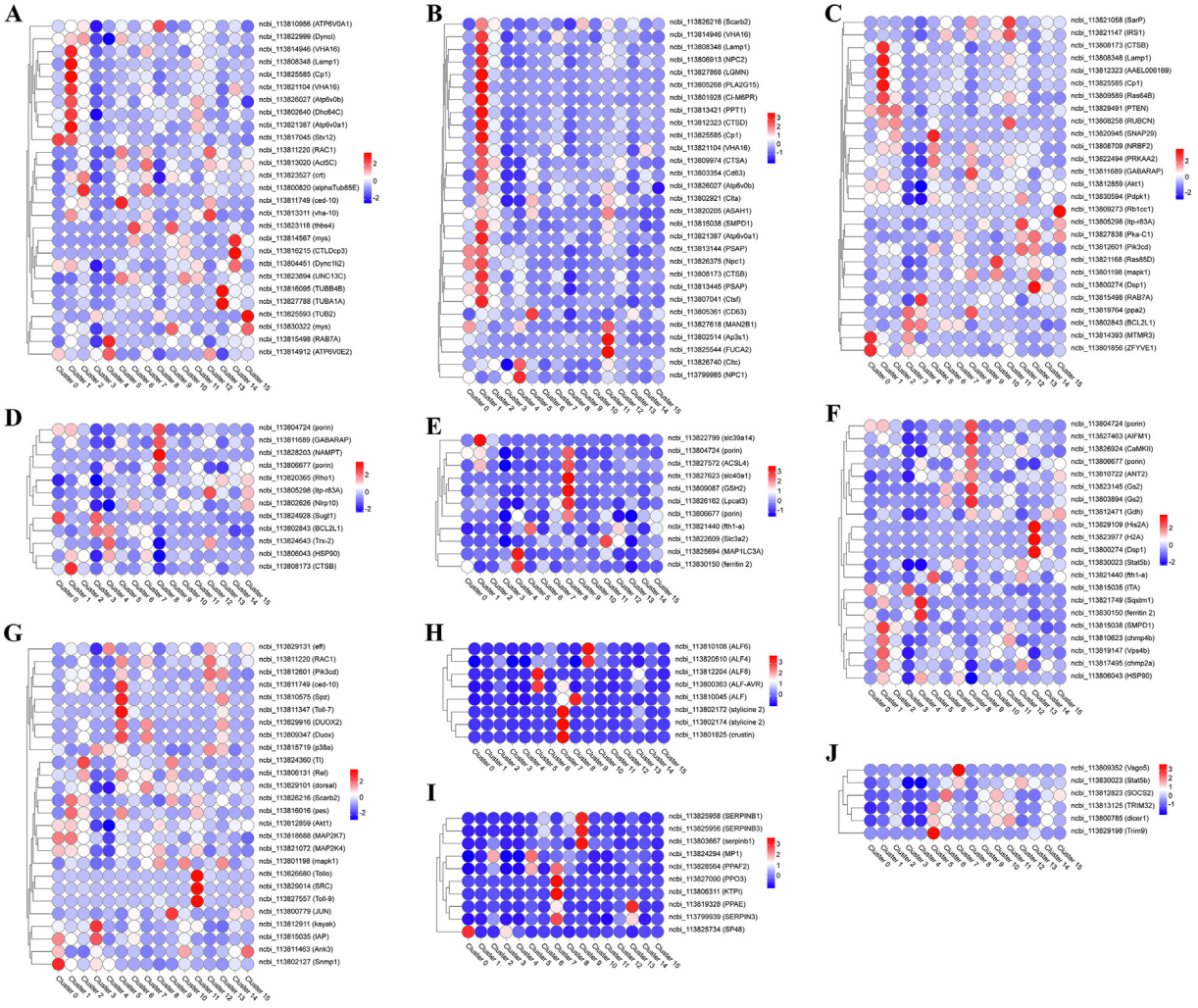

Fig. 2. Landscape of immune-related genes expression in each cluster of shrimp Oka. (A-J) Heatmap displaying the normalized expression of representative DEGs related to "phagocytosis" (A), "lysosome" (B), "autophagy" (C), "Nod-like receptor (NLR) signaling" (D), "ferroptosis" (E), "necroptosis" (F), "Toll and Imd signaling" (G), "antimicrobial peptides (AMPs)" (H), "prophenoloxidase (PPO) activation cascade" (I), and "interferon (IFN) and IFN-stimulated genes" (J) across various cell clusters in Oka. Color gradient represents the expression levels in each cluster.

differentiated branch in macrophage-like cell 1 (Fig. 3D). A total of 127 DEGs were identified between the two branches, which were visualized in a heatmap with twelve key immune regulators in the WSSV-induced branch highlighted (Fig. 3E). Following WSSV infection, antiviral genes including *Fas2*, *ZNFX1*, *Gyc76c*, *RAB11FIP5*, *MCOLN3*, *Lyz1*, *CD63*, *CTSB*, *Lamp1*, *Vago5*, *ALF*, and *Crustin* Ⅱa, were significantly upregulated in macrophage-like cell 1 (Fig. 3F). These results suggested an active antiviral response aimed to dealing with the invading virus within the macrophage-like cells of Oka.

GSEA analysis of macrophage-like cells showed that two pathways including cell adhesion molecules and lysosome were significantly enriched in macrophage-like cells following WSSV infection (Fig. 3G, Fig. 3H, Supplementary Fig. S8B, C). Among the cell adhesion molecules, all DEGs including *integrins*, *neuroligins*, *tie1*, *kielin/chordin-like protein* (*KCP*), and *Fas2*, were significantly upregulated following WSSV infection (Supplementary Fig. S8B). Most DEGs in the lysosome pathway, including *Dnase 2*, *CTSB*, and *LGMN*, were upregulated following WSSV infection, which is consistent with the results of pseudotime analysis (Supplementary Fig. S8C). WSSV could reprogram the host metabolism and hijack it for viral replication via AMPK pathway [43]. We summarized the expression changes of key genes involved in AMPK signaling and glycolysis across different clusters following WSSV infection. *AMPK*, *hypoxia inducible factor* (*HIF*), and glycolytic enzymes, including *pyruvate kinase* (*PK*), *phosphoglycerate 2 mutase 2* (*PGAM2*), and *glyceraldehyde-3-phosphate dehydrogenase* (*GAPDH*), were significantly downregulated following WSSV infection, whereas *phosphatase 2A* (*PP2A*), an inhibitory regulator of AMPK, was significantly upregulated within macrophage-like cells (Supplementary Fig. S10). These findings suggested that the macrophage-like cells in Oka likely plays a critical role in the antiviral immunity of shrimp.

Characterization of a ZAP-70 homolog and its role during viral infection in Oka

Among the DEGs in cluster 1, we identified a homolog of T-cell receptor zeta-chain-associated protein kinase 70 kDa (ZAP-70). ZAP-70 is a cytoplasmic protein tyrosine kinase that plays a critical role in initiating T-cell responses via antigen receptors [44]. The functional domains of shrimp ZAP-70 (LvZAP-70) exhibited high similarity to human ZAP-70 with high pLDDT scores proving the reliability of model prediction (Fig. 4A, Supplementary Fig. S11). Jurkat cells transfected with LvZAP-70 significantly activated the expression of human *CD69*, *CD25*, and *IL-2*, without upregulation of endogenous *ZAP-70* expression (Fig. 4B), indicating the func-

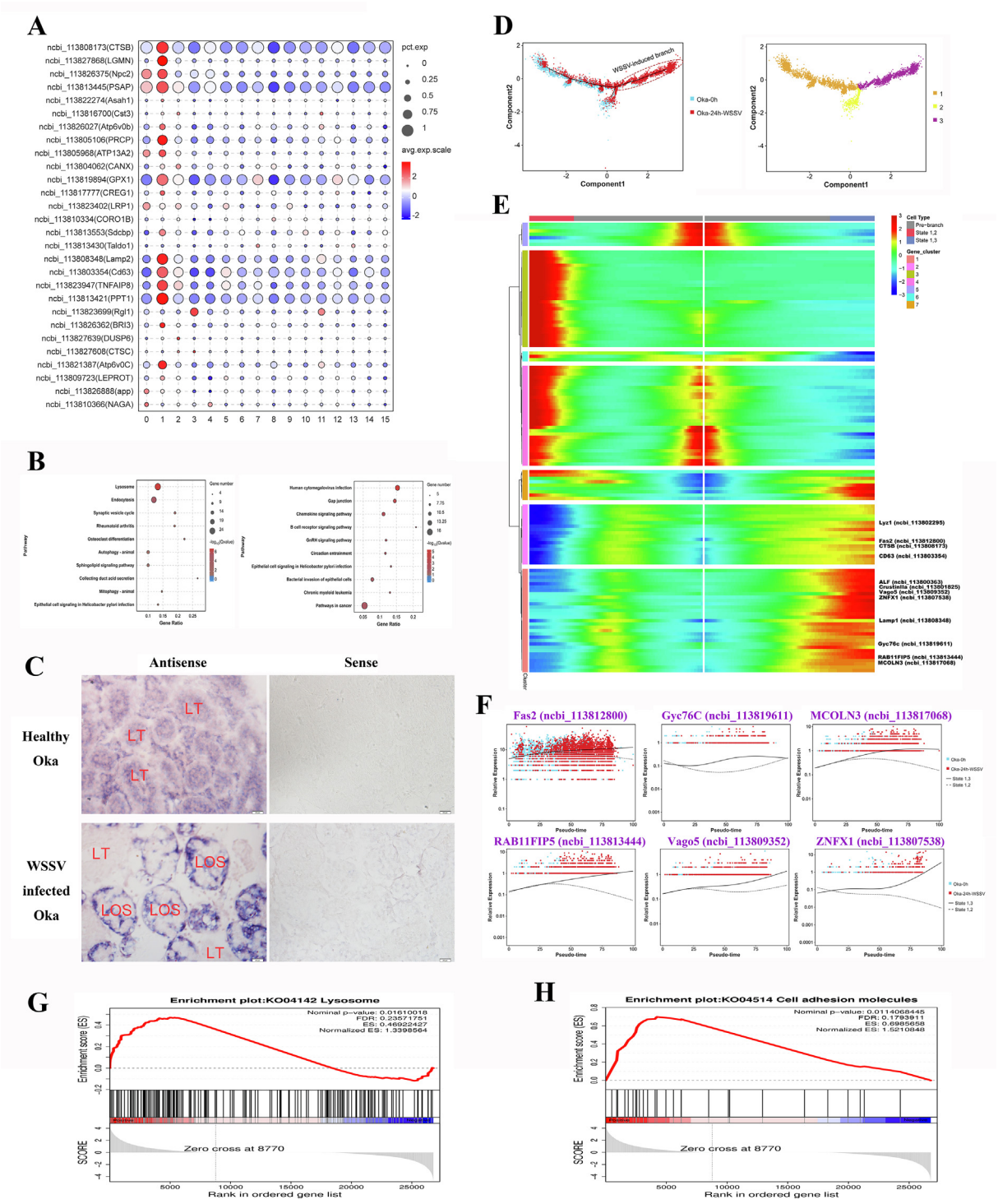

Fig. 3. Identification of macrophage-like cells in Oka of shrimp and their immune function during WSSV infection. (A) Distribution of conserved macrophage markers across multiple vertebrates in Oka cells. (B) Top 10 enriched KEGG pathways in macrophage-like cell 1 (left) and macrophage-like cell 2 (right). (C) Spatial distribution of macrophage-like cell 1 in healthy (top) and WSSV-infected (bottom) Oka. Probes: ncbi_113827868 riboprobes. Antibody: Anti-Digoxigenin-AP, Fab fragments. The positive signals were dominated located in the lymphoid tubules (LT) of healthy Oka and the lymphoid organ spheroid (LOS) of WSSV-infected Oka. Bar = 20 μm. (D) Pseudotime trajectories of macrophage-like cell 1. Distribution of macrophage-like cell 1 in healthy and WSSV-infected groups (left), and the distribution of cells in different states of differentiation in cell trajectories (right). Macrophage-like cell 1 at 0 h in the branch 1 is defined as the starting point of the differentiation trajectory. (E) A heatmap showing differentially expressed gene dynamics of macrophage-like cell 1 during WSSV infection. (F) Spline plots illustrating the expression dynamics of *Fas2*, *Gyc76c*, *MCOLN3*, *RAB11FIP5*, *Vago5* and *ZNFX1*. Dashed line indicates the WSSV-unresponsive branch, while the solid line indicates the WSSV-induced branch. (G, H) Gene set enrichment analysis (GSEA) of "lysosome" (G) and "cell adhesion molecules" (H) KEGG pathways between healthy and WSSV-infected macrophage-like cell 1 in Oka. Nominal p-value, false discovery rate (FDR), enrichment score (ES), and normalized ES are determined by the GSEA software and are indicated within each enrichment plot.

tional analogy between LvZAP-70 and human ZAP-70. *LvZAP-70* was highly expressed in Oka and significantly upregulated at 24 h following WSSV infection (Supplementary Fig. S12), indicating that the *LvZAP-70* is involved in the host response to WSSV infection.

As shown in the UMAP map and bubble plots, the *LvZAP-70* was dominantly expressed in cluster 1, with relatively high expression levels in cluster 2, 5, 9, 10, and 12. However, its expression level in cluster 1 showed no significant difference following WSSV infection (Fig. 4C, Supplementary Fig. S13). Given that cells in cluster 1 aggregated following WSSV infection, we hypothesized that WSSV infection might induce aggregation of *LvZAP-70* signals. *In-situ* hybridization revealed that *LvZAP-70* positive signals were located in the lymphoid tubules in Oka of healthy shrimp, primarily in stromal cells of the middle layer (Fig. 4D), which aligned with the spatial distribution of macrophage-like cells. *LvZAP-70* positive signals were aggregated to form large clusters in LOS following WSSV infection (Fig. 4D). The data indicated that WSSV infection induced translocation of *LvZAP-70* positive cells in Oka. Immunohistochemical assay of LvZAP-70 further confirmed that aggregation of LvZAP-70 positive cells in LOS following WSSV infection (Fig. 4E, Supplementary Fig. S14).

We further compared the expression differences between *LvZAP-70* positive and *LvZAP-70* negative cells. The *LvZAP-70* positive cells highly expressed homologs of several CD markers in vertebrate lymphocytes, including *CD16*, *CD45*, and *CD100* (Supplementary Table S7). Several genes involved in cell proliferation, antigen presentation and inflammation (e.g., *RBM10*, *ICAM-1*, *PTPN2*, *Rnf13*, *TrxG*, *ZC3H11A*, *ADAM17*, *Erap1*, and *ANKRD13*) were highly expressed in *LvZAP-70* positive cells (Supplementary Fig. S15). Furthermore, phagocytosis-related genes exhibited higher expression levels in *LvZAP-70* positive cells in Oka of both healthy (Fig. 4F) and WSSV-infected shrimp (Fig. 4G), suggesting that *LvZAP-70* positive cells in Oka might possess strong phagocytic capabilities. The presence of LvZAP-70 positive cells and their infection-induced aggregation in Oka are similar to the characteristics of pharyngeal mucosal lymphoid organ in zebrafish and other teleost [11], indicating that a putative lymphoid organ existed in crustaceans.

Cytotoxic activity of Oka cells against heterologous cells

ZAP-70 is a marker gene for T lymphocytes/NK cells. Given the absence of well-differentiated T lymphocyte in shrimp, a more plausible hypothesis is that NK-like cells might exist in Oka of shrimp. Considering that the LvZAP-70 positive cells are hard to separate at present, we used whole Oka cells for cytotoxicity detection. We found that co-culture with primary culture Oka cells induced significantly higher death rate of S2 cells (Fig. 5A). In the co-culture group, the rate of dead S2 cells was 5.08 ± 0.29%, which was significantly higher than that in the control group (2.08 ± 0.22%) ($p < 0.01$). Furthermore, tissue extract of Oka could also increase the death rate of heterologous cells, including HEK293T cell, Sf9 cell, and S2 cell. For HEK293T cells, the cell number in Oka extract group was significantly lower (Supplementary Fig. S16), and the conversion of adherent cells to suspension cells was observed in this group after PBS washing (Fig. 5B). Fluorescence microscopy observation showed more dead HEK293T cells in Oka extract group than those in the controls (Fig. 5B). For Sf9 cells, the death rate in Oka extract group (9.97 ± 0.30%) was significantly higher than those in controls (negative control, 1.43 ± 0.15%; muscle extract, 1.37 ± 0.21%; heated Oka extract, 1.73 ± 0.23%) ($p < 0.01$) (Fig. 5C, Fig. 5D). For S2 cells, the conversion of most adherent cells to suspension cells were also observed in the Oka extract group (Supplementary Fig. S17). The death rate in Oka extract group (3.80 ± 0.70%) was significantly higher than those in controls (negative control, 0.50 ± 0.10%; muscle extract, 0.50 ± 0.10%; heated Oka extract, 0.40 ± 0.01%) ($p < 0.01$) (Fig. 5E). Knockdown of *LvZAP-70* significantly suppressed the cytotoxic activity of Oka cells against heterologous cells, including Sf9 cells and S2 cells (Fig. 5F–H). For Sf9 cells, the death rate in the dsEGFP group (9.25 ± 0.13%) was significantly higher than those in the negative control (1.18 ± 0.15%) and dsZAP70 group (2.15 ± 0.24%) ($p < 0.01$) (Fig. 5G). For S2 cells, the death rate in the dsEGFP group (3.15 ± 0.17%) was also significantly higher than those in the negative control (0.43 ± 0.05%) and dsZAP70 group (1.05 ± 0.10%) ($p < 0.01$) (Fig. 5H). Additionally, *NKG2C* and *granzyme A* were expressed in cluster 1, 2, and 9 of Oka cells (Supplementary Fig. S18). These findings provided evidence for the presence of NK-like cells in Oka of shrimp.

Identification of lymphocyte precursor-like cells in Oka

Cluster 4 was identified as an analog of lymphocyte ancestor, owing to the expression of marker genes involved in pre-B cell differentiation and T cell maturation. We further performed cell type annotation using SingleR with human and murine immune cell references [45,46], revealing that cluster 4 showed the highest correlation with mammalian common lymphoid progenitor-derived cells, including B cells, T cells, NK cells and dendritic cells (Supplementary Fig. S19A, S19B). Cross-species analysis showed that evolutionary or species-specific lymphocyte (B cell and T cell) markers in vertebrates were predominantly expressed in cluster 4 and 13 (Supplementary Fig. S20). Furthermore, we analyzed the molecular features and spatial distribution of cluster 4. KEGG enrichment analysis of DEGs revealed high expression of ribosome-related genes in cluster 4 (Fig. 6A), including various ribosomal proteins (Fig. 6B, Supplementary Fig. S19C).

In-situ hybridization revealed that the positive signals of cluster 4 were scattered throughout the Oka of healthy shrimp (Fig. 6C). Notably, several reported WSSV receptors, including *rab7* and *laminin receptor* (*Lamr*) [47,48], were highly expressed in cluster 4 (Supplementary Fig. S19D), suggesting that this cluster might participate in viral recognition and engulfment. At 24 hpi, these positive signals aggregated in LOS (Fig. 6C), which were similar to those of macrophage-like cells and ZAP-70 positive cells.

Among the WSSV-responsive DEGs in cluster 4, several homologs of human CD molecules were significantly upregulated, including *CD133*, *CD49d*, *CD45*, *CD39*, and *CD21* (Fig. 6D, Supplementary Table S7). Besides, several DEGs that are involved in DNA replication and cell proliferation, including *DNA ligase 1*, *cyclin T*, *zinc finger protein 628* (*ZFP628*), and *protein tyrosine phosphatase megakaryocyte* (*PTP-MEG,* also called *PTPN9*), were upregulated following WSSV infection (Fig. 6D). Additionally, cell cycle-related DEGs, including *glycogen synthase kinase-3β* (*GSK3β*), *cullin 1*, *CREB-binding protein* (*CREBBP*), *Smad3*, *Abl*, were significantly upregulated following WSSV infection (Fig. 6E). The results indicated that WSSV infection might induce dynamic processes analogous to cell proliferation and differentiation in cluster 4.

Discussion

The emergence of lymphoid structures represents a pivotal adaptation in immune system evolution, facilitating lymphocyte development and antigen-specific responses across metazoans. The evolution of such structures is a complex topic in the animal kingdom. Although a presumptive invertebrate lymphoid organ (Oka) has been reported in shrimp based on its structural characteristics, whether it truly functions as a lymphoid organ akin to those in vertebrates remains uncertain. In contrast to the extensive diversification of immune cell types across metazoan evolution,

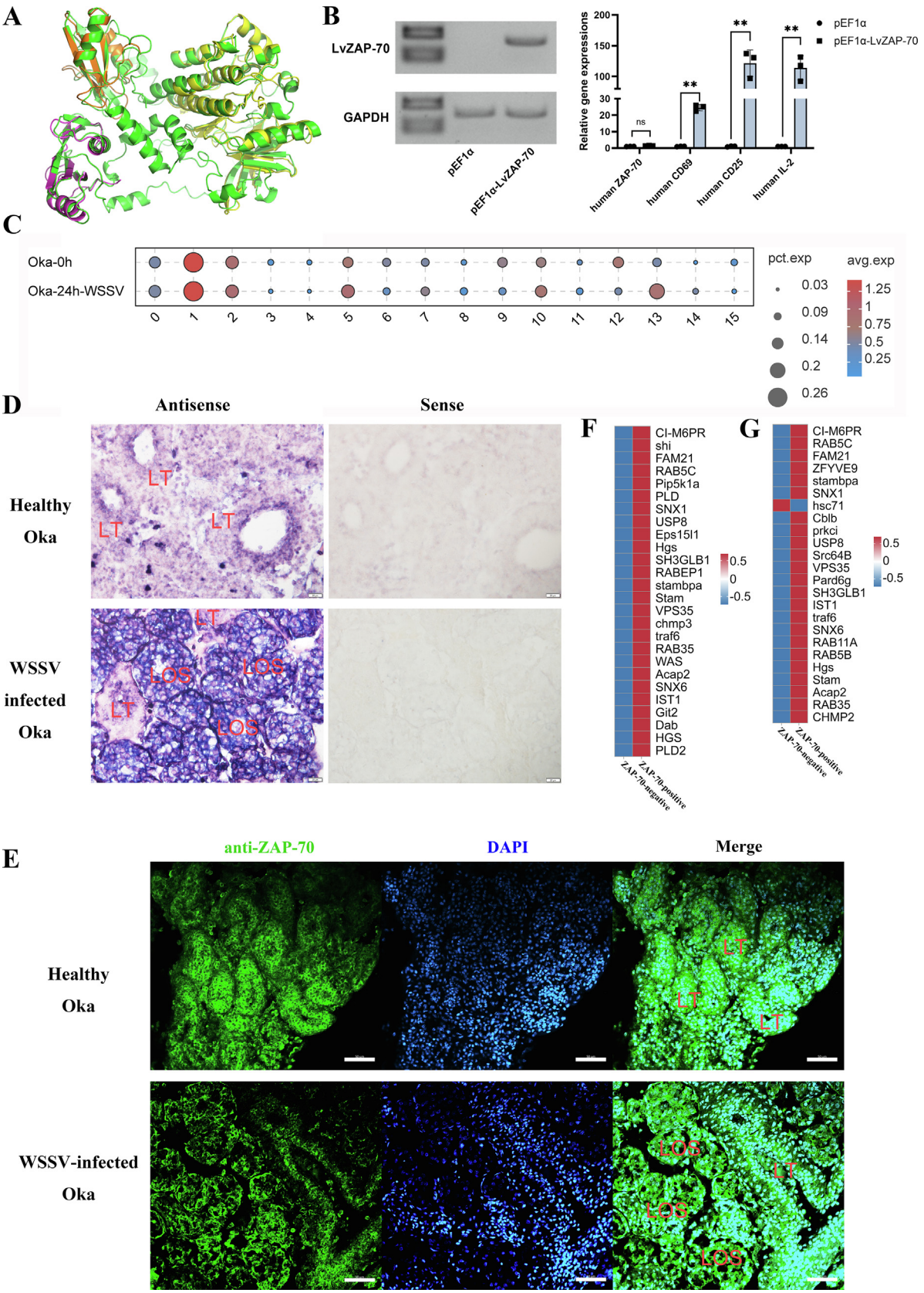
A
B
LvZAP-70
GAPDH
pEF1α
pEF1α-LvZAP-70
Relative gene expressions
pEF1α
pEF1α-LvZAP-70
ns
**
human ZAP-70
human CD69
human CD25
human IL-2
C
Oka-0h
Oka-24h-WSSV
pct.exp
avg.exp
D
Antisense
Sense
Healthy Oka
WSSV infected Oka
LT
LOS
F
G
CI-M6PR
shi
FAM21
RAB5C
Pip5k1a
PLD
SNX1
USP8
Eps15l1
Hgs
SH3GLB1
RABEP1
stambpa
Stam
VPS35
chmp3
traf6
RAB35
WAS
Acap2
SNX6
IST1
Git2
Dab
HGS
PLD2
ZFYVE9
hsc71
Cblb
prkci
Src64B
Pard6g
CHMP2
ZAP-70-positive
ZAP-70-negative
E
anti-ZAP-70
DAPI
Merge
Healthy Oka
WSSV-infected Oka

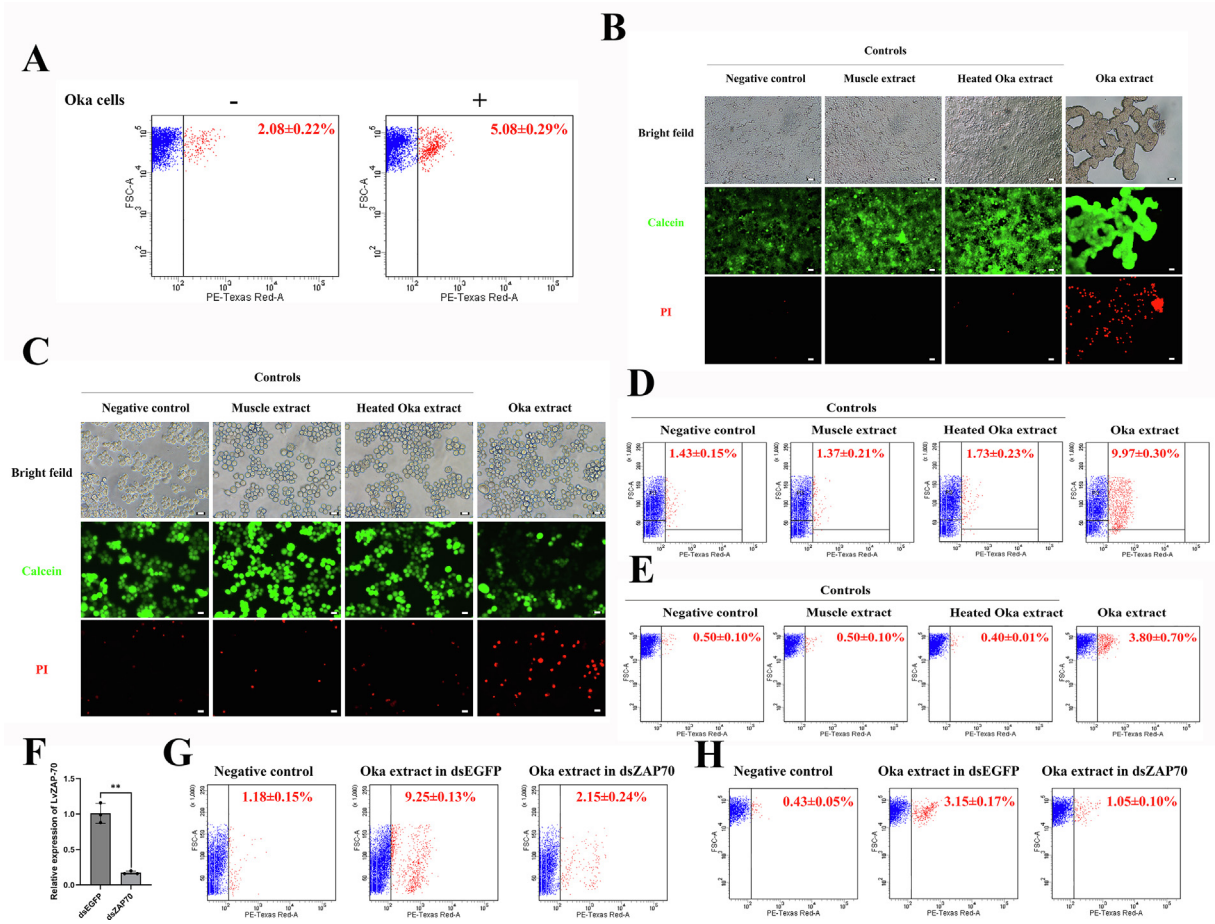

Fig. 5. Cytotoxic activity of Oka cells against heterologous cells. (A) Death rate of S2 cells after 24 h co-culture with the primary Oka cells detected via flow cytometry. "-" represents the control group, and "+" represents the co-culture group. Data shown as mean ± SE, and $p < 0.01$. (B) Microscopy observation of cytotoxic activity of Oka cells against HEK293T cell. Alive HEK293T cells exhibited green fluorescence and dead cells exhibited red fluorescence after staining with the cell viability/cytotoxicity assay kit. Bar = 20 μm. (C) Microscopy observation of cytotoxic activity of Oka cells against Sf9 cells. Alive cells were stained with green fluorescence and dead cells were stained with red fluorescence. Bar = 20 μm. (D, E) Death rate of Sf9 (D) and S2 (E) cells detected via flow cytometry. Treatments were the same as (C). Data shown as mean ± SE, and $p < 0.01$. (F-H) Role of LvZAP-70 in cytotoxic activity of Oka. (F) Inhibition efficiency of LvZAP-70 dsRNA. Expression levels of *LvZAP-70* in the Oka of dsEGFP and dsZAP70 groups at 48 h post dsRNA injection. (G, H) Death rate detection of Sf9 (G) and S2 (H) cells treated with Oka extracts from dsEGFP and dsZAP70 groups via flow cytometry. Data shown as mean ± SE, and $p < 0.01$. dsEGFP, shrimp injected with EGFP dsRNA; dsZAP70, shrimp injected with *LvZAP-70* dsRNA.

some specific proteins evolved at markedly slower rates [49]. Thus, cell-specific functional proteins are key to defining the cell subsets [14]. In the present study, we performed snRNA-seq on Oka, and conducted cross-species comparative analyses of immune cell markers between shrimp and vertebrates to elucidate evolutionary conservation patterns in invertebrate-vertebrate immunity. Histological and ultrastructural analyses showed the structural characteristics of shrimp Oka: lymphoid tubules (endothelial, stromal and capsular cells) and interstitial haemal sinuses packed with hemocytes [50]. The tubules are encased within a fibrous ECM network that confers structural integrity to the organ [8]. Our results suggested that stromal cells in Oka harbored abundant macrophage-like cells, while capsular cells in the outer layer of lymphoid tubules mediated humoral immune responses (Supplementary Fig. S3). Circulating foreign particles in hemolymph might be filtered and engulfed for degradation by macrophage-like cells within stromal cells of Oka. Subsequent presentation of processed pathogen-associated molecular patterns (PAMPs)/antigens activates humoral immune cascades in adjacent capsular cells, inducing AMP production for targeted pathogen elimination. Endothelial

Fig. 4. Identification of ZAP-70 homolog in Oka of shrimp and its function during WSSV infection. (A) Modeling prediction and alignment of human ZAP-70 and its homolog in shrimp (LvZAP-70). The predicted tertiary structures of first SH2 domain (orange), second SH2 domain (purple), and kinase domain (yellow) of LvZAP-70, along with intact human ZAP-70 (green), are shown and labeled. (B) Overexpression of LvZAP-70 activated human T cells without upregulation of human ZAP-70. The expression of *LvZAP-70* was detected by RT-PCR (left). The relative expressions of human *ZAP-70*, *CD69*, *CD25*, *IL-2* were detected by qPCR (right). Human *GAPDH* was used as an internal reference gene. Jurkat cells transfected with pEF1α-LvZAP-70 was set as pEF1α-LvZAP-70 group, and the cells transfected with pEF1α empty vector was set as control. (C) Bubble plot showing the expression level and proportion of *LvZAP-70* in each cluster of Oka. Dot size represents the fraction of cells in the cluster that express *LvZAP-70*, and intensity indicates the mean expression in expressing cells relative to other clusters. (D) Spatial distribution of *LvZAP-70* positive cells in healthy (top) and WSSV-infected (bottom) Oka via *in-situ* hybridization. Probes: *LvZAP-70* riboprobes. Antibody: Anti-Digoxigenin-AP, Fab fragments. The positive signals were dominated located in the lymphoid tubules (LT) of healthy Oka and the lymphoid organ spheroid (LOS) of WSSV-infected Oka. Bar = 20 μm. (E) Immunohistochemical localization of LvZAP-70 positive cells in Oka from healthy (top) and WSSV-infected shrimp (bottom). The LvZAP-70 positive signals were dominated located in the lymphoid tubules (LT) of healthy Oka and the lymphoid organ spheroid (LOS) of WSSV-infected Oka. Bar = 50 μm. (F, G) Heatmap displaying expression profiles of phagocytosis-related DEGs between whole *LvZAP-70*-positive and -negative cells in healthy (F) and WSSV-infected (G) Oka.

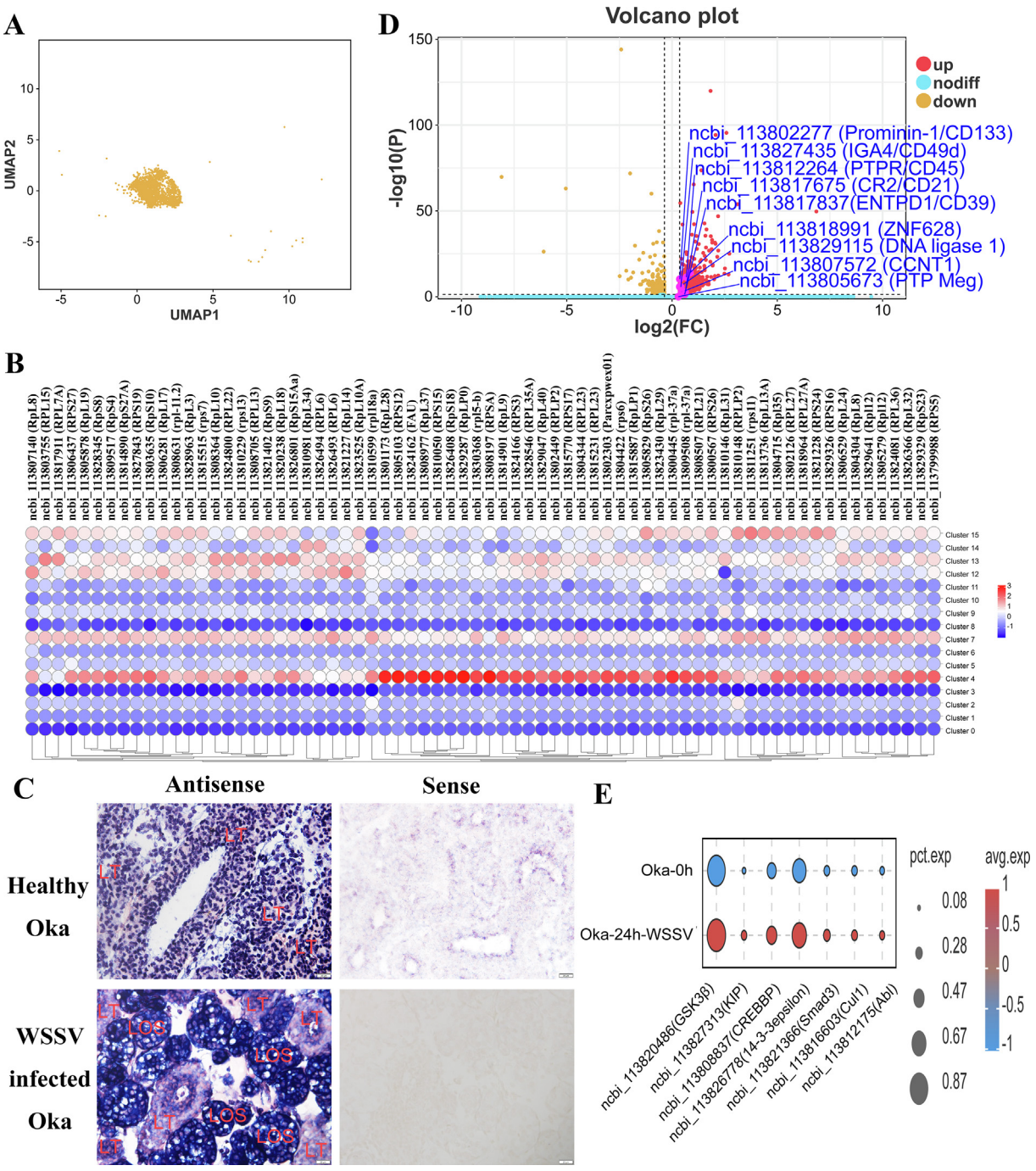

Fig. 6. Identification of lymphocyte precursor-like cells in Oka of shrimp. (A) UMAP displaying the distribution of lymphocyte precursor-like cells (cluster 4) in Oka. (B) A heatmap showing the normalized expression of representative DEGs related to "ribosome" across various cell clusters of Oka. (C) Spatial distribution of lymphocyte precursor-like cells in healthy (top) and WSSV-infected (bottom) Oka. Probes: ncbi_113818382 riboprobes. Antibody: Anti-Digoxigenin-AP, Fab fragments. The positive signals were dominated located in the lymphoid tubules (LT) of healthy Oka and the lymphoid organ spheroid (LOS) of WSSV-infected Oka. Bar = 20 μm. (D) Volcano plots of DEGs in cluster 4 between healthy and WSSV-infected shrimp. (E) Heatmap displaying expression profiles of cell cycle-related DEGs in cluster 4 between healthy and WSSV-infected shrimp.

cells included a subset of ECM-producing cells, while the remaining ECM-producing cells, together with epithelial cells, formed the outmost fibers surrounding the lymphoid tubules (Supplementary Fig. S3). As the second most abundant cellular component in Oka, further investigation into the heterogeneity of ECM-producing cells may provide additional insights into the function of epithelial cells in this tissue. Except for previously characterized cell types, snRNA-seq profiling identified novel cell lineages in Oka, including progenitor cells, lymphocyte precursor-like cells, and SLC-rich cells, which may offer new perspectives on its immunological functions. Viral challenge induced LOS formation in Oka, with lymphocyte precursor-like and macrophage-like cells as the primary cellular constituents of this structure.

Phagocytosis is a critical mechanism for multicellular organisms to clear the invading pathogens. Vertebrates maintain large populations of tissue-resident macrophages with specialized functions, yet the functional conservation of such tissue-resident analogs in invertebrates remains unclear. Macrophage-like

phagocytes have been identified in circulating hemocytes of shrimp [14]. In the present study, a population of tissue-specific macrophage-like cells were identified in Oka of shrimp. This population constitutes the largest proportion of Oka cells, which is consistent with the high phagocytic ability of Oka in shrimp [51]. In vertebrate lymphoid tissues, macrophages utilize highly developed endocytic compartments to clear microbes and apoptotic cells, mediate cellular adhesion, produce cytokines, and present antigens [52]. In shrimp Oka, endocytic and lysosomal components were highly expressed in macrophage-like cells, indicating their potential parallel functions in microbial clearance and antigen presentation similar to vertebrate macrophages. Following viral infection, macrophage-like cells in Oka migrated from the middle layer of lymphoid tubules into LOS. A high apoptotic rate has been observed in LOS [53], but whether these macrophage-like cells in Oka engaged in engulfing viral particles or virus-infected apoptotic host cells remains unclear. In macrophage-like cells, WSSV infection induced the transcription of numerous antiviral genes, including *Fas2*, *ZNFX1*, *Gyc76C*, *RAB11FIP5*, and *MCOLN3*. Fas2, an immunoglobulin superfamily adhesion molecule, mediates cell–cell adhesion during tissue morphogenesis [54,55]. ZNFX1, an interferon-inducible dsRNA sensor, activates MAVS-dependent signaling cascades to orchestrate antiviral immune defenses [56]. Gyc76C, a transmembrane guanylate cyclase receptor, triggers antimicrobial peptide synthesis to support humoral immune responses [57]. RAB11FIP5 can be elevated by viral infection and consequently regulates the NK cell function [58]. MCOLN3, a calcium-permeable channel, modulates autophagosome biogenesis [59]. The upregulation of cell adhesion molecules in macrophage-like cells, such as integrins and Fas2, is similar to the mechanism evolutionarily conserved with leukocyte trafficking in vertebrates [60]. Vertebrate macrophages also exhibit strong capacity to produce cytokines and recruit immune cells via chemokine signaling [61]. In Oka, lymphocyte precursor-like cells and macrophage-like cells translocated into LOS following WSSV infection. The discovery provides critical insights into the evolutionary origins of macrophages and lymphoid tissue specialization. However, several questions regarding these tissue-specific macrophage-like cells remain unresolved, including the antigenic specificity of their phagocytic activity, the molecular mediators of their intercellular migration, and functional analogs of cytokine signaling pathways, which will be promising avenues for further investigation.

ZAP-70 serves as a conserved biomarker for T/NK cells [44] and has been used to delineate the lymphoid architecture in zebrafish and other teleost [11,62]. Here, we identified a *ZAP-70* homolog predominantly expressed in Oka, and overexpression of this homolog in Jurkat cells led to T cell activation. In teleost, pathogen challenge induces the aggregation of ZAP-70 positive cells within lymphoid organs, where these immunologically active clusters directly participate in host defense [11,62]. Similarly, WSSV infection induced significant aggregation of LvZAP-70 positive cells into large clusters within Oka. These *LvZAP-70* positive cells exhibited elevated expressions of vertebrate lymphocyte-associated CD homologs, including *CD16*, *CD45*, and *CD100*. CD16 is a low-affinity immunoglobulin Fc receptor expressed on NK cells, mediates antibody-dependent cellular cytotoxicity (ADCC) [63]. CD45 is a transmembrane protein tyrosine phosphatase ubiquitously expressed on leukocytes, which modulates immune cell activation [64]. CD100 is a semaphorin-family protein predominantly expressed in activated T cells and hematopoietic lineages, which can facilitate activation and maturation of B cell and dendritic cell [65]. Furthermore, *LvZAP-70* positive cells showed enhanced expression of immunoregulatory genes, including *ADAM17*, *ERAP1*, *ANKRD13*, *PTPN2*, *ICAM-1*, *RNF13*, and *RBM10*. ADAM17 is a transmembrane metalloproteinase critical for inflammatory regulation and tissue homeostasis, which mediates ectodomain shedding of key immunomodulators (e.g. TNFα, IL-6R, TNF-R, L-selectin, and ICAM-1) [66]. ERAP1 is an endoplasmic reticulum-localized zinc-dependent aminopeptidase, which coordinates antigen processing through peptide trimming and presentation onto MHC molecules [67]. ICAM-1 is a canonical immunoglobulin superfamily adhesion receptor, which can facilitate leukocyte recruitment to the inflammation sites [68]. These data revealed that *LvZAP-70* positive cells in Oka might participate in the antiviral immune defense in shrimp.

To date, canonical TCR components, antigen-specific receptors or adaptive immune machinery have rarely been identified in crustaceans and other invertebrates. Therefore, the function of *LvZAP-70* positive cells in shrimp Oka is unclear. Several putative orthologues of NK cell receptors and ligands were identified in shrimp [69]. A more plausible explanation is that shrimp might possess NK-like cells, which are known to express ZAP-70. Cellular cytotoxicity reflects the ability of cells to kill other cells, which is a key effector mechanism of the immune system against viral infections. NK cells are the major cytotoxic innate lymphocytes that can lyse virally infected cells [70]. ZAP-70 is responsible for cytotoxic granule release and activation of cytotoxicity in NK cells [71]. Non-specific cytotoxic cells (NCC) in teleost are considered as evolutionary precursors of NK cells, which exhibit similar killing effects against heterologous cells [72,73]. Regarding the absence of antigen-specific receptors in shrimp, the cytotoxic analysis of Oka cells supported the possible existence of NK-like cytotoxicity rather than adaptive immunity in the vertebrate sense. NK cells kill target cells by releasing cytotoxic particles containing perforin and granzymes [74]. Granzyme A is the main components of these particles to induce the death of target cells [75]. In the present study, homologs of *granzyme A* and *NKG2C* were identified in Oka. Knockdown of *LvZAP-70* significantly suppressed the cytotoxic activity of Oka cells against heterologous cells. These data provide evidence that *LvZAP-70* positive cells shared molecular and functional parallels with NK-like cells, supporting the hypothesis that Oka functions as a lymphoid organ in shrimp. We noticed that Oka exhibited distinct cytotoxic activities against different vertebrate and insect cells. This probably correlate to different species-specific susceptibilities of the used cells. Further investigation is necessary to identify the immunological effectors and functional pathways associated with the ZAP-70 homolog in crustaceans.

Besides the *LvZAP-70* positive cells, lymphocyte precursor-like cells were identified in Oka. Across-species analysis revealed that these cells showed high correlation with vertebrate lymphocytes, and markers of the vertebrate B and T lymphocytes were predominantly expressed in these cells. In Naive T cells, a large number of idling ribosomes enable rapid translational switch to initiate T cell activation program following stimulation [76]. In the present study, high expression of ribosome-related genes was observed in lymphocyte precursor-like cells of Oka. DNA ligase 1 catalyzes the process to complete DNA replication and repair [77]. PTP-MEG (PTPN9) regulates zebrafish erythropoiesis and proliferation by activation of STAT proteins [78]. In this study, above genes involved in DNA replication, cell cycle, and cell proliferation were significantly upregulated following WSSV infection. CD133 (Prominin-1) is a conserved stem cell biomarker in lymphoid tissues [79]. CD49d (integrin α4) regulates leukocyte adhesion, migration, and survival [80]. CD45 is a lymphocyte common antigen and critically regulates immune cells activation [64]. CD39 governs functions of regulatory T cells (Tregs) and conventional $CD4^+$/$CD8^+$ T lymphocytes [81,82]. Complement receptor CD21, predominantly expressed on B cells, mediates B cell activation and antigen presentation [83]. Homologs of these CD molecules were upregulated in lymphocyte precursor-like cells of Oka. Functionally, the lymphocyte precursor-like cells aggregated together with *LvZAP-70* positive cells following viral infection. The results

suggest that WSSV infection could induce dynamic processes analogous to lymphocyte progenitor proliferation and lymphocyte differentiation in these lymphocyte precursor-like cells.

In addition to cellular analogs, the structural organization of Oka mirrors fundamental features of vertebrate lymphoid tissues (Supplementary Fig. S1), indicating evolutionary parallels in immune system architecture. A defining characteristic of structured lymphoid aggregates, such as the lymph nodes, Peyer's patches, or tonsils, is the spatial arrangement of immune cells within a reticulated stromal framework, which facilitates immune cell interactions [84]. Analogously, the Oka in shrimp features reticular fibers surrounding its lymphoid tubules [8] and vascular networks. This is very similar to those in teleost lymphoid tissues, which enables efficient immune cell trafficking [11]. Similar to the nemausean lymphoid organ in teleost, the presence of LvZAP-70 positive cells in Oka of shrimp and their pathogen-responsive aggregation suggested conserved mechanisms between these structures. Lymphoid tissue lining the gut tube is a universal feature of vertebrates. Primary lymphoid tissue in some species resides in the typhlosole, an invagination of the gut wall [85]. In sharks, gut-associated lymphoid structures are located in two specialized regions: the Leydig's organ near the esophageal junction, and the spiral valve in the posterior intestine [86]. The Oka in shrimp is positioned ventrolateral at the junction of the anterior stomach and foregut (Supplementary Fig. S1) [87]. Antigen-driven hyperplasia was observed in shark GALT [88], and similarly, shrimp Oka enlarges in response to pathogen exposure [89,90]. Collectively, the Oka in shrimp shares key hallmarks with vertebrate lymphoid organs, including anatomical location, pathogen-induced structural remodeling, and the presence of molecular homologs and functional similarity of NK-like cytotoxicity.

The origin, migration and evolution of cells in Oka are key scientific questions worth exploring. Vertebrate lymph organs have mesoderm-dominated origins with minor contributions from endoderm [91]. To our knowledge, there are still no reports on the developmental origin of cells in Oka. Here we identified progenitor cells with probable proliferating ability in Oka. This type of cells might be one of the origins of Oka cells. However, it is still unclear which type or which types of cells are differentiated from progenitor cells. Although other stem cells such as those in hematopoietic tissue (HPT) have been reported in shrimp [92], no evidence shows the association between them and the cells in Oka. In vertebrates, a large amount of microvasculature and lymphatic capillary benefit the traffic and homing of immune cells [93]. In shrimp, the circulatory system is open. The circulating hemolymph is pumped from the heart via subgastric artery into Oka, and the foreign materials in hemolymph are filtered within Oka [51]. Based on our results, immune cells in Oka might translocate from the lymphoid tubules into nearby haemal sinuses to remove the foreign materials through the formation of LOS. At present, researchers believe that invertebrates do not possess true lymphoid tissues or adaptive immune cells. In addition to Oka in crustaceans, mollusks and echinoderms have evolved specialized lymphoid-like tissues. These tissues include hematopoietic tissue, white body in mollusks, and axial organ, Tiedemann's bodies in echinoderms [94,95]. They function in cell recruitment, pathogen clearance, and localized immune responses. However, the lack of sufficient comparative analysis of lymphoid-like tissues in other invertebrate taxa limited our understanding on the evolution of lymphoid-like tissues across animal kingdom.

Conclusion

In summary, we performed snRNA-seq on the invertebrate lymphoid organ (Oka) in *L. vannamei*, and characterized the immune functions of major cell types to trace its evolutional commonality with vertebrate lymphoid organs. We identified tissue-specific macrophage-like cells and lymphocyte precursor-like cells in Oka, which migrated into aggregates following WSSV infection. Additionally, a homolog of the conserved lymphocyte marker ZAP-70 colocalizes in LOS with macrophage-like cells and lymphocyte precursor-like cells following WSSV infection. Functional analyses provide evidence to confirm that Oka functions as a lymphoid organ in shrimp. However, further investigations are needed to resolve several questions, including the proliferative capacity of Oka cells, the ontogenetic origin of the organ, the functional roles of SLC-rich cells, and the mechanistic interplay between ZAP-70 homologs and antiviral effectors.

Compliance with ethics requirements

The methods were performed in accordance with relevant guidelines and regulations and approved by the Animal Ethics Committee [2020(37)] at Institute of Oceanology, Chinese Academy of Sciences.

Data availability

Single-nucleus RNA-seq data have been deposited at NCBI (accession numbers: PRJNA1185480) and are publicly available as of the date of publication.

CRediT authorship contribution statement

Mingzhe Sun: Funding acquisition, Investigation, Methodology, Visualization, Writing – original draft, Writing – review & editing. **Shihao Li:** Funding acquisition, Investigation, Writing – review & editing. **Yuan Liu:** Investigation, Writing – review & editing. **Fuhua Li:** Conceptualization, Funding acquisition, Supervision, Writing – review & editing.

Declaration of competing interest

The authors declare that they have no known competing financial interests or personal relationships that could have appeared to influence the work reported in this paper.

Acknowledgments

This study was supported by the Strategic Priority Research Program of the Chinese Academy of Sciences (XDB0730201), the Natural Science Foundation of China (32102830), the China Agriculture Research System-48 (CARS-48), and the Taishan Scholars Program. We thank Mr. Zhanyuan Yang for assistance in structure prediction and visualization. This research was supported by Oceanographic Data Center, IOCAS.

Appendix A. Supplementary data

Supplementary data to this article can be found online at https://doi.org/10.1016/j.jare.2025.11.018.

References

[1] Boehm T, Bleul CC. The evolutionary history of lymphoid organs. Nat Immunol 2007;8(2):131–5. doi: https://doi.org/10.1038/ni1435.
[2] Boehm T, Swann JB. Origin and evolution of adaptive immunity. Annu Rev Anim Biosci 2014;2:259–83. doi: https://doi.org/10.1146/annurev-animal-022513-114201.
[3] Neely HR, Flajnik MF. Emergence and evolution of secondary lymphoid organs. Annu Rev Cell Dev Bi 2016;32:693–711. doi: https://doi.org/10.1146/annurev-cellbio-111315-125306.

[4] Boehm T, Hess I, Swann JB. Evolution of lymphoid tissues. Trends Immunol 2012;33(6):315–21. doi: https://doi.org/10.1016/j.it.2012.02.005.
[5] Boehm T, Swann JB. Thymus involution and regeneration: two sides of the same coin? Nat Rev Immunol 2013;13(11):831–8. doi: https://doi.org/10.1038/nri3534.
[6] Lazado CC, Caipang CMA. Mucosal immunity and probiotics in fish. Fish Shellfish Immun 2014;39(1):78–89. doi: https://doi.org/10.1016/j.fsi.2014.04.015.
[7] Oka M. Studies on *Penaeus orientolis* KISHINOUYE-VIII: Structure of the newly found lymphoid organ. Nippon Suisan Gakk 1969;35:245–50.
[8] Duangsuwan P, Phoungpetchara I, Tinikul Y, Poljaroen J, Wanichanon C, Sobhon P. Histological and three dimensional organizations of lymphoid tubules in normal lymphoid organ of *Penaeus monodon*. Fish Shellfish Immun 2008;24(4):426–35. doi: https://doi.org/10.1016/j.fsi.2007.12.011.
[9] Li SH, Lv XJ, Li FH, Xiang JH. Characterization of a lymphoid organ specific anti-lipopolysaccharide factor from shrimp reveals structure-activity relationship of the LPS-binding domain. Front Immunol 2019;10. doi: https://doi.org/10.3389/fimmu.2019.00872.
[10] Bonami JR, Lightner DV, Redman RM, Poulos BT. Partial characterization of a Togavirus (Lovv) associated with histopathological changes of the lymphoid organ of *Penaeid shrimps*. Dis Aquat Organ 1992;14(2):145–52. doi: https://doi.org/10.3354/dao014145.
[11] Resseguier J, Nguyen-Chi M, Wohlmann J, Rigaudeau D, Salinas I, Oehlers SH, et al. Identification of a pharyngeal mucosal lymphoid organ in zebrafish and other teleosts: tonsils in fish? Sci Adv 2023;9(44):eadj0101. doi: https://doi.org/10.1126/sciadv.adj0101.
[12] Cui C, Tang XQ, Xing J, Sheng XZ, Chi H, Zhan WB. Single-cell RNA-seq uncovered hemocyte functional subtypes and their differentiational characteristics and connectivity with morphological subpopulations in. Front Immunol 2022;13. doi: https://doi.org/10.3389/fimmu.2022.980021.
[13] Söderhäll I, Fasterius E, Ekblom C, Söderhäll K. Characterization of hemocytes and hematopoietic cells of a freshwater crayfish based on single-cell transcriptome analysis. Iscience 2022;25(8). doi: https://doi.org/10.1016/j.isci.2022.104850.
[14] Yang P, Chen Y, Huang Z, Xia H, Cheng L, Wu H, et al. Single-cell RNA sequencing analysis of shrimp immune cells identifies macrophage-like phagocytes. eLife 2022;11:e80127. doi: https://doi.org/10.7554/eLife.80127.
[15] Zhu W, Yang C, Chen X, Liu Q, Li Q, Peng M, et al. Single-cell ribonucleic acid sequencing clarifies cold tolerance mechanisms in the pacific white shrimp (*Litopenaeus vannamei*). Front Genet 2021;12:792172. doi: https://doi.org/10.3389/fgene.2021.792172.
[16] Sun Y, Li F, Xiang J. Analysis on the dynamic changes of the amount of WSSV in Chinese shrimp *Fenneropenaeus chinensis* during infection. Aquaculture 2013;376–379:124–32. doi: https://doi.org/10.1016/j.aquaculture.2012.11.014.
[17] Mu H, Chen J, Huang W, Huang G, Deng M, Hong S, et al. OmicShare tools: a zero-code interactive online platform for biological data analysis and visualization. iMeta 2024;3(5):e228. doi: https://doi.org/10.1002/imt2.228.
[18] Abramson J, Adler J, Dunger J, Evans R, Green T, Pritzel A, et al. Accurate structure prediction of biomolecular interactions with AlphaFold 3. Nature 2024;630(8016):493–500. doi: https://doi.org/10.1038/s41586-024-07487-w.
[19] Sun M, Li S, Jin S, Li X, Xiang J, Li F. A novel TRIM9 protein promotes NF-κB activation through interacting with LvIMD in shrimp during WSSV infection. Front Immunol 2022;13. doi: https://doi.org/10.3389/fimmu.2022.819881.
[20] Trębacz H, Barzycka A. Mechanical properties and functions of elastin: an overview. Biomolecules 2023;13(3). doi: https://doi.org/10.3390/biom13030574.
[21] Zhu F, Gao J, Qiao K, Xiao S, Bai X, Kang M, et al. Identification of BmELP as an interaction partner of Bmtutl-519 in the silkworm, *Bombyx mori*. J Asia-Pac Entomol 2021;24(3):521–8. doi: https://doi.org/10.1016/j.aspen.2021.03.005.
[22] Ventura T, Fitzgibbon QP, Battaglene SC, Elizur A. Redefining metamorphosis in spiny lobsters: molecular analysis of the phyllosoma to puerulus transition in Sagmariasus verreauxi. Sci Rep 2015;5(1):13537. doi: https://doi.org/10.1038/srep13537.
[23] Cordova AF, Ritchie C, Böhnert V, Li L. Human SLC46A2 is the dominant cGAMP importer in extracellular cGAMP-sensing macrophages and monocytes. ACS Cent Sci 2021;7(6):1073–88. doi: https://doi.org/10.1021/acscentsci.1c00440.
[24] Jia D, Chen S, Bai P, Luo C, Liu J, Sun A, et al. Cardiac resident macrophage-derived legumain improves cardiac repair by promoting clearance and degradation of apoptotic cardiomyocytes after myocardial infarction. Circulation 2022;145(20):1542–56. doi: https://doi.org/10.1161/CIRCULATIONAHA.121.057549.
[25] Bai P, Lyu L, Yu T, Zuo C, Fu J, He Y, et al. Macrophage-derived legumain promotes pulmonary hypertension by activating the MMP (matrix metalloproteinase)-2/TGF (transforming growth factor)-β1 signaling. Arterioscl Throm Vas 2019;39(4):e130–45. doi: https://doi.org/10.1161/atvbaha.118.312254.
[26] Yeh MS, Liu CH, Hung CW, Cheng W. cDNA cloning, identification, tissue localisation, and transcription profile of a transglutaminase from white shrimp, *Litopenaeus vannamei*, after infection by Vibrio alginolyticus. Fish Shellfish Immun 2009;27(6):748–56. doi: https://doi.org/10.1016/j.fsi.2009.09.006.
[27] Wang YC, Chang PS, Chen HY. Tissue expressions of nine genes important to immune defence of the Pacific white shrimp *Litopenaeus vannamei*. Fish Shellfish Immun 2007;23(6):1161–77. doi: https://doi.org/10.1016/j.fsi.2007.04.004.
[28] Karlsson M, Zhang C, Méar L, Zhong W, Digre A, Katona B, et al. A single–cell type transcriptomics map of human tissues. Sci Adv 2021;7(31):eabh2169. doi: https://doi.org/10.1126/sciadv.abh2169.
[29] Iram T, Ramirez-Ortiz Z, Byrne MH, Coleman UA, Kingery ND, Means TK, et al. Megf10 is a receptor for C1Q that mediates clearance of apoptotic cells by astrocytes. J Neurosci 2016;36(19):5185–92. doi: https://doi.org/10.1523/jneurosci.3850-15.2016.
[30] Yao X, He Z, Qin C, Deng X, Bai L, Li G, et al. SLC2A3 promotes macrophage infiltration by glycolysis reprogramming in gastric cancer. Cancer Cell Int 2020;20:503. doi: https://doi.org/10.1186/s12935-020-01599-9.
[31] Lee RD, Munro SA, Knutson TP, LaRue RS, Heltemes-Harris LM, Farrar MA. Single-cell analysis identifies dynamic gene expression networks that govern B cell development and transformation. Nat Commun 2021;12(1):6843. doi: https://doi.org/10.1038/s41467-021-27232-5.
[32] Gil-Krzewska A, Wood SM, Murakami Y, Nguyen V, Chiang SCC, Cullinane AR, et al. Chediak-Higashi syndrome: Lysosomal trafficking regulator domains regulate exocytosis of lytic granules but not cytokine secretion by natural killer cells. J Allergy Clin Immunol 2016;137(4):1165–77. doi: https://doi.org/10.1016/j.jaci.2015.08.039.
[33] Zawerton A, Yao B, Yeager JP, Pippucci T, Haseeb A, Smith JD, et al. De novo SOX4 variants cause a neurodevelopmental disease associated with mild dysmorphism. Am J Hum Genet 2019;104(2):246–59. doi: https://doi.org/10.1016/j.ajhg.2018.12.014.
[34] Malhotra N, Narayan K, Cho OH, Sylvia KE, Yin C, Melichar H, et al. A network of high-mobility group box transcription factors programs innate interleukin-17 production. Immunity 2013;38(4):681–93. doi: https://doi.org/10.1016/j.immuni.2013.01.010.
[35] Chen Z, Tayyab M, Yao D, Aweya Jude J, Zheng Z, Zhao X, et al. Cell death in crustacean immune defense. Rev Aquacult 2024;17(1). doi: https://doi.org/10.1111/raq.12976.
[36] Li FH, Xiang JH. Recent advances in researches on the innate immunity of shrimp in China. Dev Comp Immunol 2013;39(1–2):11–26. doi: https://doi.org/10.1016/j.dci.2012.03.016.
[37] Li CZ, Wang S, He JG. The two NF-kappa B pathways regulating bacterial and WSSV infection of shrimp. Front Immunol 2019;10:26. doi: https://doi.org/10.3389/fimmu.2019.01785.
[38] Braulke T, Carette JE, Palm W. Lysosomal enzyme trafficking: from molecular mechanisms to human diseases. Trends Cell Biol 2024;34(3):198–210. doi: https://doi.org/10.1016/j.tcb.2023.06.005.
[39] Yang MC, Shi XZ, Yang HT, Sun JJ, Xu L, Wang XW, et al. Scavenger receptor C mediates phagocytosis of White spot syndrome virus and restricts virus proliferation in shrimp. PLoS Pathog 2016;12(12):e1006127. doi: https://doi.org/10.1371/journal.ppat.1006127.
[40] Li XC, Li SH, Sun MZ, Yu Y, Zhang XJ, Xiang JH, et al. A newly identified NLR-like gene participates in bacteria and virus infection possibly through regulating hemocytes apoptosis in shrimp. Dev Comp Immunol 2022;132:104395. doi: https://doi.org/10.1016/j.dci.2022.104395.
[41] Zhu Z, Wu X, Zhang J, Zhu M, Tian M, Zhao P. Advances in understanding ferroptosis mechanisms and their impact on immune cell regulation and tumour immunotherapy. Discov Oncol 2025;16(1):153. doi: https://doi.org/10.1007/s12672-025-01911-x.
[42] Gao J, Zhao B-R, Zhang H, You Y-L, Li F, Wang X-W. Interferon functional analog activates antiviral Jak/Stat signaling through integrin in an arthropod. Cell Rep 2021;36(13). doi: https://doi.org/10.1016/j.celrep.2021.109761.
[43] Zhang P, Fu H-J, Lv L-X, Liu C-F, Han C, Zhao X-F, et al. WSSV exploits AMPK to activate mTORC2 signaling for proliferation by enhancing aerobic glycolysis. Commun Biol 2023;6(1):361. doi: https://doi.org/10.1038/s42003-023-04735-z.
[44] Chan AC, Iwashima M, Turck CW, Weiss A. ZAP-70: a 70 kd protein-tyrosine kinase that associates with the TCR ζ chain. Cell 1992;71(4):649–62. doi: https://doi.org/10.1016/0092-8674(92)90598-7.
[45] Heng TS, Painter MW. The immunological genome project: networks of gene expression in immune cells. Nat Immunol 2008;9(10):1091–4. doi: https://doi.org/10.1038/ni1008-1091.
[46] Schmiedel BJ, Singh D, Madrigal A, Valdovino-Gonzalez AG, White BM, Zapardiel-Gonzalo J, et al. Impact of genetic polymorphisms on human immune cell gene expression. Cell 2018;175(6):1701–1715.e16. doi: https://doi.org/10.1016/j.cell.2018.10.022.
[47] Liu W-J, Li Y-C, Kou G-H, Lo C-F. Laminin receptor in shrimp is a cellular attachment receptor for White spot syndrome virus. PLoS One 2016;11(6):e0156375. doi: https://doi.org/10.1371/journal.pone.0156375.
[48] Sritunyalucksana K, Wannapapho W, Lo CF, Flegel TW. PmRab7 is a VP28-binding protein involved in white spot syndrome virus infection in shrimp. J Virol 2006;80(21):10734–42. doi: https://doi.org/10.1128/jvi.00349-06.
[49] Jayaraman V, Toledo-Patiño S, Noda-García L, Laurino P. Mechanisms of protein evolution. Protein Sci 2022;31(7):e4362.
[50] Duangsuwan P, Thaweethamsawee P, Sobhon P. Ultrastructure of cells constituting lymphoid tubules and circulating hemocytes in Penaeus monodon. Fish Shellfish Immun 2022;131:1040–50. doi: https://doi.org/10.1016/j.fsi.2022.10.038.
[51] Rusaini OL. Insight into the lymphoid organ of penaeid prawns: a review. Fish Shellfish Immun 2010;29(3):367–77. doi: https://doi.org/10.1016/j.fsi.2010.05.011.
[52] den Haan JM, Martinez-Pomares L. Macrophage heterogeneity in lymphoid tissues. Semin Immunopathol 2013;35(5):541–52. doi: https://doi.org/10.1007/s00281-013-0378-4.

[53] Anggraeni MS, Owens L. The haemocytic origin of lymphoid organ spheroid cells in the penaeid prawn *Penaeus monodon*. Dis Aquat Organ 2000;40 (2):85–92. doi: https://doi.org/10.3354/dao040085.
[54] Waghmare I, Kango-Singh M. Loss of cell adhesion increases tumorigenic potential of polarity deficient scribble mutant cells. PLoS One 2016;11(6): e0158081. doi: https://doi.org/10.1371/journal.pone.0158081.
[55] Laiouar S, Berns N, Brech A, Riechmann V. RabX1 organizes a late endosomal compartment that forms tubular connections to lysosomes consistent with a kiss and run mechanism. Curr Biol 2020;30(7):1177–1188.e5. doi: https://doi.org/10.1016/j.cub.2020.01.048.
[56] Wang Y, Yuan S, Jia X, Ge Y, Ling T, Nie M, et al. Mitochondria-localised ZNFX1 functions as a dsRNA sensor to initiate antiviral responses through MAVS. Nat Cell Biol 2019;21(11):1346–56. doi: https://doi.org/10.1038/s41556-019-0416-0.
[57] Iwashita S, Suzuki H, Goto A, Oyama T, Kanoh H, Kuraishi T, et al. A receptor guanylate cyclase, Gyc76C, mediates humoral, and cellular responses in distinct ways in Drosophila immunity. Front Immunol 2020;11. doi: https://doi.org/10.3389/fimmu.2020.00035.
[58] Bradley T, Peppa D, Pedroza-Pacheco I, Li D, Cain DW, Henao R, et al. RAB11FIP5 expression and altered Natural Killer cell function are associated with induction of HIV broadly neutralizing antibody responses. Cell 2018;175 (2):387–399.e17. doi: https://doi.org/10.1016/j.cell.2018.08.064.
[59] Lei Y, Klionsky DJ. MCOLN3/TRPML3 bridges the regulation of autophagosome biogenesis by PtdIns3P and the calcium channel. Autophagy 2023;19 (2):377–8. doi: https://doi.org/10.1080/15548627.2022.2148808.
[60] Su Y, Yin X. The molecular mechanism of macrophages in response to mechanical stress. Ann Biomed Eng 2024. doi: https://doi.org/10.1007/s10439-024-03616-8.
[61] Mantovani A, Gray PA, Van Damme J, Sozzani S. Macrophage-derived chemokine (MDC). J Leukoc Biol 2000;68(3):400–4.
[62] Dalum AS, Kraus A, Khan S, Davydova E, Rigaudeau D, Bjørgen H, et al. 3D imaging of the zebrafish gill-associated lymphoid tissue (GIALT) reveals a novel lymphoid structure, the amphibranchial lymphoid tissue. Front Immunol 2021;12. doi: https://doi.org/10.3389/fimmu.2021.769901.
[63] Stern-Ginossar N, Mandelboim O. Chapter eleven - Receptors on NK cells. In: Lotze MT, Thomson AW, editors. Natural Killer Cells. San Diego: Academic Press; 2010. p. 155–68.
[64] Altin JG, Sloan EK. The role of CD45 and CD45-associated molecules in T cell activation. Immunol Cell Biol 1997;75(5):430–45. doi: https://doi.org/10.1038/icb.1997.68.
[65] Zhang Y, Liu B, Ma Y, Jin B. Sema 4D/CD100-plexin B is a multifunctional counter-receptor. Cell Mol Immunol 2013;10(2):97–8. doi: https://doi.org/10.1038/cmi.2012.65.
[66] Scheller J, Chalaris A, Garbers C, Rose-John S. ADAM17: a molecular switch to control inflammation and tissue regeneration. Trends Immunol 2011;32 (8):380–7. doi: https://doi.org/10.1016/j.it.2011.05.005.
[67] Maben Z, Arya R, Rane D, An WF, Metkar S, Hickey M, et al. Discovery of selective inhibitors of endoplasmic reticulum aminopeptidase 1. J Med Chem 2020;63(1):103–21. doi: https://doi.org/10.1021/acs.jmedchem.9b00293.
[68] Bui TM, Wiesolek HL, Sumagin R. ICAM-1: a master regulator of cellular responses in inflammation, injury resolution, and tumorigenesis. J Leukoc Biol 2020;108(3):787–99. doi: https://doi.org/10.1002/jlb.2mr0220-549r.
[69] Zheng L, Byadgi OV, Rakhshaninejad M, Nauwynck H. Putative orthologues of natural killer cell receptors and ligands in shrimp. Dev Comp Immunol 2025;171:105459. doi: https://doi.org/10.1016/j.dci.2025.105459.
[70] Prager I, Watzl C. Mechanisms of natural killer cell-mediated cellular cytotoxicity. J Leukoc Biol 2019;105(6):1319–29. doi: https://doi.org/10.1002/JLB.MR0718-269R.
[71] Hideshima T, Ogiya D, Liu JY, Harada T, Kurata K, Bae J, et al. Immunomodulatory drugs activate NK cells via both Zap-70 and cereblon-dependent pathways. Leukemia 2021;35(1):177–88. doi: https://doi.org/10.1038/s41375-020-0809-x.
[72] Huang Y, Chen Z, Zhang J, Amoah K, Asiedu B, Cai J, et al. Novel C-type lectin mediated non-specific cytotoxic cells killing activity through NCCRP-1 in nile tilapia (*Oreochromis niloticus*). Fish Shellfish Immun 2024;149:109594. doi: https://doi.org/10.1016/j.fsi.2024.109594.
[73] Huang Y, Zheng Q, Wang Z, Tang J, Lu Y, Qin Q, et al. Fish natural killer enhancing factor-A (NKEF-A) enhance cytotoxicity of nonspecific cytotoxic cells against bacterial infection. Mol Immunol 2021;133:184–93. doi: https://doi.org/10.1016/j.molimm.2021.02.017.
[74] Lim YS, Lee AG, Jiang X, Scott JM, Cofie A, Kumar S, et al. NK cell-derived extracellular granzyme B drives epithelial ulceration during HSV-2 genital infection. Cell Rep 2023;42(4). doi: https://doi.org/10.1016/j.celrep.2023.112410.
[75] Lieberman J. Granzyme a activates another way to die. Immunol Rev 2010;235 (1):93–104. doi: https://doi.org/10.1111/j.0105-2896.2010.00902.x.
[76] Wolf T, Jin W, Zoppi G, Vogel IA, Akhmedov M, Bleck CKE, et al. Dynamics in protein translation sustaining T cell preparedness. Nat Immuno 2020;21 (8):927–37. doi: https://doi.org/10.1038/s41590-020-0714-5.
[77] Williams JS, Tumbale PP, Arana ME, Rana JA, Williams RS, Kunkel TA. High-fidelity DNA ligation enforces accurate Okazaki fragment maturation during DNA replication. Nat Commun 2021;12(1):482. doi: https://doi.org/10.1038/s41467-020-20800-1.
[78] Bu Y, Su F, Wang X, Gao H, Lei L, Chang N, et al. Protein tyrosine phosphatase PTPN9 regulates erythroid cell development through STAT3 dephosphorylation in zebrafish. J Cell Sci 2014;127(12):2761–70. doi: https://doi.org/10.1242/jcs.145367.
[79] Moreno-Londoño AP, Robles-Flores M. Functional roles of CD133: more than stemness associated factor regulated by the microenvironment. Stem Cell Rev Rep 2024;20(1):25–51. doi: https://doi.org/10.1007/s12015-023-10647-6.
[80] Shanafelt TD, Geyer SM, Bone ND, Tschumper RC, Witzig TE, Nowakowski GS, et al. CD49d expression is an independent predictor of overall survival in patients with chronic lymphocytic leukaemia: a prognostic parameter with therapeutic potential. Br J Haematol 2008;140(5):537–46. doi: https://doi.org/10.1111/j.1365-2141.2007.06965.x.
[81] Timperi E, Barnaba V. CD39 regulation and functions in T cells. Int J Mol Sci 2021;22(15). doi: https://doi.org/10.3390/ijms22158068.
[82] Moesta AK, Li X-Y, Smyth MJ. Targeting CD39 in cancer. Nat Rev Immunol 2020;20(12):739–55. doi: https://doi.org/10.1038/s41577-020-0376-4.
[83] Roozendaal R, Carroll MC. Complement receptors CD21 and CD35 in humoral immunity. Immunol Rev 2007;219:157–66. doi: https://doi.org/10.1111/j.1600-065X.2007.00556.x.
[84] Katakai T, Hara T, Lee JH, Gonda H, Sugai M, Shimizu A. A novel reticular stromal structure in lymph node cortex: an immuno-platform for interactions among dendritic cells, T cells and B cells. Int Immunol 2004;16(8):1133–42. doi: https://doi.org/10.1093/intimm/dxh113.
[85] Finstad J, Papermaster BW, Good RA. Evolution of the immune response. II. Morphologic studies of the origin of the thymus and organized lymphoid tissue. Lab Invest 1964;13:490–512.
[86] Hansen JD, Zapata AG. Lymphocyte development in fish and amphibians. Immunol Rev 1998;166:199–220. doi: https://doi.org/10.1111/j.1600-065x.1998.tb01264.x.
[87] Cruz-Suárez LE, González-Félix ML, Chapter P-V. Digestive anatomy and physiology of shrimp. In: Kumar V, editor. Nutrition and Physiology of Fish and Shellfish, 16. Academic Press; 2025. p. 691–741.
[88] Hart S, Wrathmell AB, Harris JE. Ontogeny of gut-associated lymphoid tissue (GALT) in the dogfish *Scyliorhinus canicula* L. Vet Immunol Immunopathol 1986;12(1–4):107–16. doi: https://doi.org/10.1016/0165-2427(86)90115-7.
[89] Lu Y, Loh PC. Infectivity studies of rhabdovirus in the penaeid blue shrimp. Aquac Int 1994;2(2):123–7. doi: https://doi.org/10.1007/BF00128806.
[90] Shao MY, Zhang ZF, Kang KH, Chen ZT, Kim JM. The study on the cytology and histochemistry of lymphoid organ spheroids in Penaeus chinensis. Aquaculture 2004;240(1):463–71. doi: https://doi.org/10.1016/j.aquaculture.2004.02.027.
[91] Semo J, Nicenboim J, Yaniv K. Development of the lymphatic system: new questions and paradigms. Development 2016;143(6):924–35. doi: https://doi.org/10.1242/dev.132431.
[92] Söderhäll I. Crustacean hematopoiesis. Dev Comp Immunol 2016;58:129–41. doi: https://doi.org/10.1016/j.dci.2015.12.009.
[93] Stritt S, Koltowska K, Mäkinen T. Homeostatic maintenance of the lymphatic vasculature. Trends Mol Med 2021;27(10):955–70. doi: https://doi.org/10.1016/j.molmed.2021.07.003.
[94] Smith VJ, Accorsi A, Malagoli D. Chapter 1 - Hematopoiesis and Hemocytes in Pancrustacean and Molluscan Models. In: Malagoli D, editor. The Evolution of the Immune System. Academic Press; 2016. p. 1–28.
[95] Ziegler A, Faber C, Bartolomaeus T. Comparative morphology of the axial complex and interdependence of internal organ systems in sea urchins (Echinodermata: Echinoidea). Front Zool 2009;6(1):10. doi: https://doi.org/10.1186/1742-9994-6-10.